

## HIGHLIGHTS

- Investigating the applicability of an efficient urban climate model for planning liveable cities
- Good agreement between TARGET model results and spatially distributed private weather station data
- Sensitivity testing indicates key variables affecting urban heat: canyon shape and concrete parameters
- Substantial air temperature reduction (up to 5.2 °C) with increasing blue-green land cover across city
- Model coupling with pedestrian count data supports people-centric spatial planning of urban spaces

# Investigating the efficacy of a fast urban climate model for spatial planning of green and blue spaces for heat mitigation

Jixuan Chen<sup>1)</sup>, Peter M. Bach<sup>2)3)\*</sup>, Kerry A. Nice<sup>4)</sup>, João P. Leitão<sup>1)</sup>

<sup>1)</sup> Swiss Federal Institute of Aquatic Science & Technology (Eawag), Überlandstrasse 133, 8600 Dübendorf  
ZH, Switzerland

<sup>2)</sup> Institute of Environmental and Process Engineering, Eastern Switzerland University of Applied Sciences  
(OST), Oberseestrasse 10, 8640 Rapperswil SG, Switzerland

<sup>3)</sup>Department of Civil Engineering, Monash University, Clayton, VIC 3800, Australia<sup>4)</sup> Transport, Health,  
and Urban Systems Research Lab, Faculty of Architecture, Building, and Planning, University of Melbourne,  
Melbourne, VIC 3010, Australia

\* Corresponding author email: [peterbach@gmail.com](mailto:peterbach@gmail.com)

## HIGHLIGHTS

- Investigating the applicability of an efficient urban climate model for planning liveable cities
- Good agreement between TARGET model results and spatially distributed private weather station data
- Sensitivity testing indicates key variables affecting urban heat: canyon shape and concrete parameters
- Substantial air temperature reduction (up to 5.2 °C) with increasing blue-green land cover across city
- Model coupling with pedestrian count data supports people-centric spatial planning of urban spaces

## ABSTRACT

Problems caused by urban heat have prompted the exploration of urban greenery and blue spaces for heat mitigation. Various numerical models can simulate heat-related processes, but their use as support-tools to urban planners remains underexplored, particularly at the city-scale, due to high computational demand and complexity of such models. This study investigates the spatial relationships between urban heat, urban form and urban green and blue spaces with the fast climate model TARGET (The Air-temperature Response to

28 Green/blue-infrastructure Evaluation Tool), which only requires minimal inputs of standard meteorological  
29 data, land cover and building geometry data. Using the City of Zurich as our case study, we: (i) validated the  
30 TARGET model against air temperature measurements from private sensor networks, (ii) performed a  
31 sensitivity analysis to identify key variables affecting urban heat, and (iii) investigated urban heat relationships  
32 with blue-green cover at locations frequented by pedestrians. Presence of urban green and blue spaces across  
33 the region shows potential for reducing local air temperatures by up to 5.2 °C (with urban forest). Investigating  
34 this relationship at different locations in the city revealed key districts that should potentially be targeted for  
35 reduction of pedestrian heat-impacts, due to their high pedestrian traffic, fewer green and blue spaces and high  
36 daytime air temperatures. Our results not only provide insights into the cooling effect of different amounts of  
37 green and blue features in the urban environment, but also demonstrates the application and integration  
38 potential of simplified models like TARGET to support the planning of more liveable future cities.

39

#### 40 **KEYWORDS**

41 urban climate; urban greenery; green spaces; blue spaces; urban planning; model-based planning-support;  
42 crowd-sourced data; meteoblue; Netatmo; TARGET

## 43 **1. INTRODUCTION**

44 The summer of 2024 is confirmed to be the hottest ever recorded since reliable global measurements began,  
45 surpassing the previous benchmark set just a year earlier in 2023 (Copernicus, 2024). However, the trend  
46 towards more frequent heatwaves due to climate change will continue, regardless of our efforts to mitigate, as  
47 warned by the World Metrological Organization (United Nations, 2022). IPCC (2021) reported that the goal  
48 to limit global warming below 2 or 1.5 °C is unachievable unless emissions of greenhouse gases are  
49 significantly reduced in future decades. In urban settings, extreme heat has negative impacts on human health  
50 (Ebi et al., 2021; Nicholls et al., 2008), livelihoods and infrastructure (IPCC, 2022; Topham, 2022). The 2022  
51 heatwave in Europe has resulted in over 60,000 heat-related deaths, estimated from the Eurostat mortality  
52 database (Ballester et al., 2023). The economic loss due to heat-induced productivity drop amounts to 0.3 - 0.5%  
53 of European GDP historically and is predicted to increase fivefold if no measures are in place by 2060 (García-  
54 León et al., 2021). As such, we must prepare for a hotter climate.

55 Cities are particularly vulnerable to weather extremes and research interest in urban climate has rapidly  
56 increased in the past decade with a focus on urban heat and its mitigation (Masson et al., 2020). The negative  
57 impacts of heatwaves are exacerbated in cities as a result of rapid urbanisation (Solecki & Marcotullio, 2013).  
58 The modification of land cover from natural to artificial materials like concrete and asphalt changes the thermal  
59 properties of the urban surface and the urban water cycle (Manoli et al., 2019; Oke, 1987), leading to increased  
60 energy storage, reduced evapotranspiration and decreased ventilation. With more than half of the world's  
61 population living in urban areas (United Nations, 2019), the capacity of the population and urban services to  
62 cope with urban heat has become a major concern. The translation of knowledge from urban climate research  
63 to urban planning and policymaking is key to develop practical solutions and alleviate stress on urban  
64 environment and populations (Kwok & Ng, 2021).

65 Research efforts for urban heat mitigation have predominantly focused on innovative pavement designs (Wang  
66 et al., 2021), reflective materials (Santamouris & Fiorito, 2021) (should be used with caution as they may  
67 negatively impact pedestrian thermal comfort, e.g., Middel et al., 2020; Schneider et al., 2023) and increasing  
68 greenery (Wong et al., 2021). It has been demonstrated that one of the best methods for urban outdoor cooling  
69 is to increase vegetation cover (Probst et al., 2022). In fact, evapotranspiration from both green and blue spaces

70 is primarily relevant for pedestrian-level air temperature reduction (Gunawardena et al., 2017). While the  
71 cooling effects of urban green and blue spaces has been extensively studied by methods of field measurements  
72 (Broadbent, Coutts, Tapper, Demuzere, et al., 2018; Skoulika et al., 2014; C. Yu & Hien, 2006) , remote  
73 sensing (Gobatti et al., 2023; Vahmani & Jones, 2017; Z. Yu et al., 2017) and numerical modelling (Gromke  
74 et al., 2015; Tsoka et al., 2018) at multiple scales (Krayenhoff et al., 2021), spatially explicit city-scale  
75 simulation remains rare, and it is yet to be explored utilizing modelling tools to evaluate different scenarios to  
76 support city-wide planning of green and blue spaces.

77 Given the heterogeneity of the urban fabric and function, the local climates across different locations within a  
78 city can exhibit significant variability. Understanding how urban heat is distributed over an urban area is  
79 important to identify mitigation measures, given limited resources. Numerical modelling, compared to field  
80 observations, is a more viable approach to study the interactions between cities and climate, elucidating the  
81 role of different processes and facilitating informed urban heat mitigation planning (Oke et al., 2017).

82 To study urban climate at finer spatial resolutions (< 1 km), energy balance models (e.g. Town Energy Balance  
83 TEB: Masson, 2000) have been extensively used until early 2000s, before computational fluid dynamics (CFD)  
84 models gained popularity in this research discipline (Toparlar et al., 2017). Perhaps the most popular CFD-  
85 based tool used in urban climate studies is ENVI-met (Bruse & Fleer, 1998), which captures all processes of  
86 surface-air-vegetation interactions and has been extensively validated in many studies over the last two decades  
87 (e.g., Elraouf et al., 2022; Ozkeresteci et al., 2003; Salata et al., 2016). Other CFD models include SOLENE-  
88 microclimat, Ansys® Fluent and OpenFOAM® (Matsson, 2023; Musy et al., 2015; Weller et al., 1998). More  
89 recently, the large-eddy simulation (LES, a branch of CFD) model PALM-4U (Maronga et al., 2020) has been  
90 increasingly used for investigating urban climates at very fine scales (Anders et al., 2023; Geletič et al., 2021).  
91 Emerging models like CityFFD (Mortezazadeh et al., 2022) leverages graphics processing units (GPUs) for  
92 parallel computation. Despite their prowess, CFD-based models often still require higher computing power  
93 and runtime, suffer from improper parameterisation (Bouzouidja et al., 2021) and inaccuracy (Jamei et al.,  
94 2019) and are limited to micro- to district-scale simulations due to their complexity. Less complex are models  
95 such as RayMan (Matzarakis et al., 2007) and SOLWEIG (Lindberg et al., 2008) that calculate radiation fluxes  
96 in urban areas up to neighbourhood-scale, or SUEWS (Järvi et al., 2011a), which models surface energy and  
97 hydrological fluxes at local-scale. Despite some authors having claimed that these modelling tools can be used

98 to support planning and ultimately testing of urban heat mitigation options, only a few studies have been  
99 presented on this aspect (Alves et al., 2022; Musy et al., 2015). In recent years, with the growing demand for  
100 supporting the planning of heat mitigation strategies, more simplified models have been developed, focusing  
101 on incorporating representations of trees, vegetation and soil processes. VTUF-3D (K. A. Nice et al., 2018) is  
102 an urban microclimate model designed for assessing the effects of green spaces on human thermal comfort. It  
103 is detailed and spatially distributed, but still requires high computational cost. The Urban Tethys-Chloris  
104 (UT&C) (Meili et al., 2020) is a fully-coupled energy and water balance model that has a strong focus on the  
105 biophysics and ecophysiology of vegetation. It is less expensive in terms of computational effort, but due to  
106 its 1-D nature, spatial modelling at larger scales remains difficult. The Urban Weather Generator (UWG)  
107 (Bueno et al., 2013) couples building energy and urban canyon models and calculates the canopy layer air  
108 temperature and humidity. UWG focuses on the urban heat island and is not spatialised in its original form.  
109 Assessment of urban heat at higher spatial resolution at district- to city-scale with a more human-centric  
110 method is urged (Nazarian et al., 2022). TARGET (Broadbent et al., 2019) is an urban climate modelling tool  
111 that builds upon the Local-Scale Urban Meteorological Parameterisation Scheme (LUMPS) (Grimmond &  
112 Oke, 2002). It is a rapid spatial model that calculates pedestrian-level air temperatures with minimal inputs  
113 and effort in parameter setting. Its representation of urban greenery is through different land cover types,  
114 linking directly to the urban form, making it suitable for supporting urban planning practices.

115 Despite the proposed urban climate models, a very small number of studies has focused on the accuracy of  
116 modelling results across city-wide scales (Broadbent et al., 2019), and on the main parameters' influence of  
117 modelling results. This can be explained by (i) the complexity of the models and their consequently large  
118 computational demand, and (ii) the need for spatially distributed temperature data, which is not frequently  
119 available or accessible. As mentioned above, recently proposed, simplified microclimate models, such as  
120 TARGET, make city-scale simulations feasible, whereas citizen science and the advent of private sensor  
121 networks, e.g. weather stations, create the possibility to assess the validity of urban climate models at a city  
122 scale (e.g. Potgieter et al., 2021). Such models also offers potential to assess and improve the walkability (e.g.  
123 Jia & Wang, 2021; Mouada et al., 2019) on a city-scale, or to facilitate active transport route choice. The  
124 relative simplicity of such models also allows for detailed sensitivity analysis of model parameters to quantify  
125 the uncertainty of obtained results.

126 Based on the few research challenges described above, we address the following research questions in this  
127 study:

- 128 • Are simplified urban climate models like TARGET able to capture the spatial variability of daytime air  
129 temperature in a city?
- 130 • What are the important characteristics of the built environment that impacts urban heat?
- 131 • How much cooling can green and blue spaces provide in the modelling scheme?
- 132 • How can simplified models like TARGET be useful in supporting city-wide planning of green and blue  
133 spaces for heat mitigation?

134 The following study presents methods to enable the effective use of TARGET (our selected model of choice)  
135 in supporting urban planning for heat mitigation. We specifically evaluate its performance against spatially-  
136 distributed air temperature measurements from private networks and understand, through sensitivity analysis,  
137 key model parameters that influence urban heat. With this, we then demonstrate the potential of currently  
138 existing urban green and blue spaces across the case study city to mitigate urban heat and how the coupling of  
139 urban climate modelling with spatial pedestrian traffic count data can assess and identify opportunities for  
140 more strategic and human-centric planning of heat mitigation measures across urban areas.

## 141 **2. MATERIALS AND METHODS**

### 142 *2.1 Overview of the selected microclimate model*

143 The Air-Temperature Response to Green/blue-infrastructure Evaluation Tool (TARGET) (Broadbent et al.,  
144 2019) was developed to be an efficient model to estimate surface temperature and street-level (2 m above  
145 ground) air temperature and to assess impacts of urban greenery and water features. TARGET can be applied  
146 at specific locations or on a spatial grid (minimum resolution of 30 m recommended for surface temperature  
147 and 100 m for air temperature). This section serves as a reiteration of the modelling approaches of the TARGET  
148 model. Further specific details of the model are explained in Broadbent et al. (2019) including its individual  
149 sub-models for different land cover types.

150 The model requires three data inputs: (1) land cover, (2) building geometry, and (3) meteorological forcing  
151 data. Land cover input should contain fractions of roofs, concrete, road, dry grass, irrigated grass, trees, and  
152 water. Average building height and street width for each grid cell are also part of the input data to determine



153 the shape of the urban canyon. Meteorological data (typically from a nearby reference point e.g., an airport or  
 154 open field) include: *incoming shortwave radiation* ( $K_{\downarrow}$  [ $\text{W m}^{-2}$ ]), *incoming longwave radiation* ( $L_{\downarrow}$  [ $\text{W m}^{-2}$ ]),  
 155 *relative humidity* (RH [%]), *air temperature* ( $T_a$  [ $^{\circ}\text{C}$ ]) and *wind speed* ( $U_z$  [ $\text{m s}^{-1}$ ]). Longwave radiation can be  
 156 modelled in TARGET if not available. The meteorological input is used as forcing data for the model, local  
 157 conditions are simulated based on the influence of the building and urban characteristics. The schematic of  
 158 TARGET canyon set-up and the structure of TARGET sub-models can be found in Supplementary Information  
 159 (SI) S1.

160 TARGET comprises a series of sub-models that calculate the radiation balance, energy balance and, eventually,  
 161 surface temperature for each surface type with the input meteorological forcing data. At its intended resolution,  
 162 the shape and density of buildings and vegetation can be generalised into a sky view factor (SVF) for a given  
 163 mix of urban forms as shown in Eq. (1), and in turn used to calculate available net energy ( $R_{n,i}$ ) that reaches  
 164 the urban surface of type  $i$ , as shown in Eq. (2).

$$165 \quad SVF = \begin{cases} \left[ 1 + \left( \frac{H}{W^*} \right)^2 \right]^{\frac{1}{2}} - \frac{H}{W^*} & \text{for ground} \\ \frac{1}{2} \left( 1 + \frac{W^*}{H} - \left[ 1 + \left( \frac{W^*}{H} \right)^2 \right]^{\frac{1}{2}} \right) & \text{for wall} \\ 1 & \text{for roof} \end{cases} \quad (1)$$

$$166 \quad R_{n,i} = \left( K_{\downarrow} (1 - \alpha_i) + \epsilon_i (L_{\downarrow} - \sigma T_{surf,i,[t-2]}^4) \right) SVF_i \quad (2)$$

167 where  $H$  is building height [m],  $W^*$  is average street width minus tree width [m],  $\alpha_i$  is surface albedo [-],  $\epsilon_i$  is  
 168 surface emissivity [-],  $\sigma$  is the Stefan-Boltzmann constant ( $=5.67 \times 10^{-8} \text{ W m}^{-2} \text{ K}^{-4}$ ), and  $T_{surf,i,[t-2]}$  is the modelled  
 169 surface temperature from two time steps back [ $^{\circ}\text{C}$ ]. Albedo and emissivity parameters for different land cover  
 170 types have preset values in TARGET, but can be adjusted by users.

171 This net energy is then partitioned into components of sensible, latent, and ground storage fluxes according to  
 172 Eq. (3). The ground storage flux ( $Q_{G,i}$ ) varies through the Objective Hysteresis Model (OHM) (see Grimmond  
 173 & Oke, 2002) with different coefficient values ( $a_1$ ,  $a_2$ , and  $a_3$ ) to account for different amounts of heat capacity  
 174 for different surface types.

$$Q_{G,i} = R_{n,i}a_{1,i} + \left(\frac{\partial R_{n,i}}{\partial t}\right)a_{2,i} + a_{3,i} \quad (3)$$

The force-restore method (Jacobs et al., 2000) is used to calculate the surface temperature change between time steps for each land cover type. As an efficient alternative to the multi-layer conduction method that is commonly used in other climate models, the force-restore method assumes the complex surfaces to be a thin surface layer on top of a deep soil layer, both with uniform vertical temperatures. The calculation then uses a forcing terms driven by the ground flux  $Q_{G,i}$  to heat the surface, and a restore term from the deep soil that restrains the forcing term, as written in Eq. (4).

$$\frac{\partial T_{surf,i}}{\partial t} = \frac{Q_{G,i}}{C_i D} - \frac{2\pi}{\tau} (T_{surf,i,[t-1]} - T_{m,i,[t-1]}) \quad (4)$$

where  $C_i$  is the volumetric heat capacity [ $\text{J m}^{-3} \text{K}^{-1}$ ],  $D$  is the damping depth of the diurnal temperature wave [m],  $\tau$  is the period (86400 s), and  $T_m$  is the average soil temperature [ $^{\circ}\text{C}$ ], which is calculated using Eq. (5).

$$\frac{\partial T_{m,i}}{\partial t} = \frac{\Delta Q_{G,i}}{C_i D_y} \quad (5)$$

where  $D_y$  is the damping depth for the annual temperature cycle ( $= D\sqrt{365}$ ) [m].

Tree canopy is considered as part of the urban canopy in the model, i.e. trees are modelled at roof height, which allows for a simplified representation of radiation reduction through shading. The surface temperature of trees is assumed to be equal to the meteorological air temperature data, which is proven to be a realistic and efficient estimation ( $r^2 = 0.98$ , RMSE = 1.17  $^{\circ}\text{C}$ ) (Broadbent, Coutts, Nice, Demuzere, Krayenhoff, et al., 2019). The surface beneath trees is assumed to be representative of ground-level surfaces in the canyon.

There is a separate model that addresses these aspects for water surfaces to ensure reliable results because the OHM-force-restore method tend to substantially over-predict daytime surface water temperatures. The water model resolves the surface energy balance of the water layer considering the absorption of shortwave radiation by water and is designed for small inland water bodies with depths of 0.1 – 1 m.

In the end, for each location (specific point or cell in the grid), surface temperatures are aggregated based on its land cover fractions using Eq. (6). Above-canopy air temperature  $T_b$  [ $^{\circ}\text{C}$ ] is calculated from the meteorological input and wind characteristics. Air temperature is then determined through the surface

200 temperature and  $T_b$  by two resistances as shown in Eq. (7). Heat from building walls are taken into account,  
 201 but anthropogenic heat fluxes are not modelled explicitly.

$$202 \quad T_{surf} = \sum_i^8 (T_{surf,i} F_i) \quad (6)$$

$$203 \quad T_{ac} = \frac{\sum_i^7 (T_{surf,i} c_s F_i) + \left[ \frac{T_{surf,roof} F_{roof}}{\left(\frac{1}{c_s} + \frac{1}{c_a}\right)} \right] + (T_b c_a W)}{\sum_i^7 (c_s F_i) + \left[ \frac{F_{roof}}{\left(\frac{1}{c_s} + \frac{1}{c_a}\right)} \right] + (c_a W)} \quad (7)$$

204 where  $F_i$  is the 2-D fractional coverage of surface  $i$  in the canyon [-],  $c_s$  is the conductance from the surface to  
 205 the urban canopy layer [ $\text{m s}^{-1}$ ], and  $c_a$  is the conductance from the urban canopy layer to the above-canopy  
 206 layer [ $\text{m s}^{-1}$ ]. Heat transfer from roofs are approximated by two resistances in series.

207

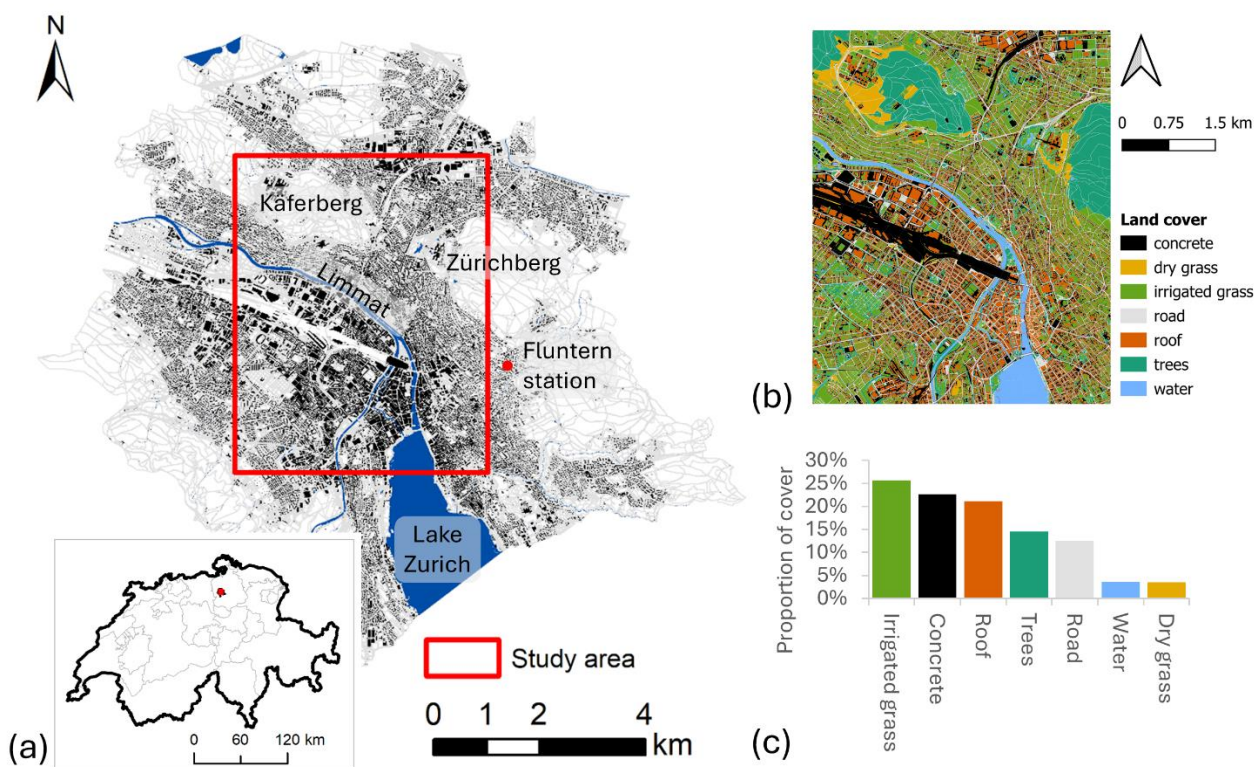
208 As part of its development, the model has been validated for a 14-day period for land cover surface temperature  
 209 at a spatial resolution of 30 m and for a 2-day period for air temperature at a spatial resolution of 100 m. The  
 210 model is intended for short simulations of days to weeks (i.e. a heatwave) with clear sky conditions and not  
 211 yet validated for longer period.

212 The model is carefully designed to balance between simplicity and accuracy with the aim of providing good  
 213 predictions of street-level air temperature with minimal input and skill requirement. It thus does not account  
 214 for the horizontal advection, so the predicted cooling impacts of heat mitigation measures are likely to be the  
 215 maximum potential, which is rather useful for practitioners and policymakers to evaluate different options.  
 216 The model is open-source and scripted in both Java and Python. Ongoing work involves integrating it to a  
 217 QGIS plugin that allows direct application and visualisation of modelling results, which will make the model  
 218 highly accessible to non-expert users.

## 219 **2.2 Case study description**

220 We selected a study area of 28.8  $\text{km}^2$  spanning the core centre of the City of Zurich in Switzerland (shown in  
 221 Figure 1) to conduct our study. The area has a diverse land-use composition, with gardens and parks scattered  
 222 on a principal amount of mixed commercial, offices, and residential zones. Some light industries are located

223 along the major railway and also on the outskirts of the study region. The river of *Limmat* flows through the  
 224 area from *Lake Zurich*. Two large, vegetated areas north of the river, the *Käferberg* and *Zürichberg* are also  
 225 included in this study area. Consequently, the area includes all TARGET land cover classes, with the most  
 226 prevalent being concrete, roof, and irrigated grass, as shown in Figure 1.  
 227 On the temporal aspect, to be consistent with the purpose of the model (it is intended for short periods like  
 228 heatwaves) and, at the same time, provide greater practical value, we selected a short period of warmer  
 229 temperatures, when a level 3 (considerable danger, daily mean temperature  $\geq 25$  °C for at least three  
 230 consecutive days) heat wave warning was issued for lowlands throughout Switzerland. to demonstrate the  
 231 heat mitigation benefits that greenery can provide during typical hotter days in the City of Zurich in summer.



232  
 233 **Figure 1.** Location of the selected study area, percentages of TARGET land cover classes in the study area (a – left),  
 234 land cover map of the study area (b – upper right) and the proportions of land cover types (c – lower right).

## 235 2.3 Data collection and pre-processing

### 236 2.3.1 Spatial data

237 Land cover data were obtained from the local planning authority and resulted from recent official surveying  
 238 (ARE, 2019). As a pre-processing step, the data were re-classified into the seven land cover types used in the

239 TARGET model (shown in Figure 1(b) and (c)). Digital surface model (DSM) data of 0.5 m resolution  
240 (swisstopo, 2020) was used to calculate building heights and street widths according to (Lindberg et al., 2015).  
241 Land cover fractions, building heights, and street widths were aggregated into 100 m grid cells and used as  
242 input to the TARGET model.

243 The global map of local climate zones (LCZs) (Demuzere et al., 2022) was used to group the numerous private  
244 weather stations, thus allowing the comparison of model accuracy under different urban environmental  
245 conditions.

246 For demographic indicators, we used pedestrian and bicycle traffic counts gathered by the Zurich civil  
247 engineering office (Stadt Zürich, 2023) to describe how frequently different areas are traversed by citizens.  
248 There are 20 of automatic counting stations in the study area that count both incoming and outgoing  
249 pedestrians and cyclists every 15 minutes. Only one station was kept for one model grid cell of 100 m in the  
250 case where multiple stations sit in the same cell, resulting in a total of 18 locations. This study used hourly  
251 averaged pedestrian and bicycle count in the warmer hours (12:00 – 18:00) as a metric to judge the traffic  
252 volume (see Figure 2(b)) in the post spatial analysis.

### 253 *2.3.2 Meteorological data*

254 As another input to the TARGET model, meteorological data were obtained from Fluntern meteorological  
255 station (556 m a.s.l.) located nearest to the study area (MeteoSwiss, 2023). The data comprises global  
256 (shortwave) radiation, incoming longwave radiation, air temperature, relative air humidity, wind speed, and  
257 pressure at station level, measured at 10-minute intervals for four days from 2023/07/08 to 2023/07/11. The  
258 data were then resampled into 15-minute intervals for to match the temporal resolution of measured data for  
259 model evaluation.

260 To be able to evaluate the spatial output of air temperature results from the model, local air temperature  
261 measurements were desired as data from standard weather stations do not have sufficient spatial resolution to  
262 be compared with the modelling results. Spatially distributed data from the climate service and data provider  
263 meteoblue, which is measured by a quality-controlled Internet of Things (IoT) measurement network  
264 (meteoblue, 2024), were available for the City of Zurich. Air temperature measurements at 15-minute intervals  
265 from 41 of such stations were obtained for the period studied. Additionally, citizen-contributed data were  
266 collected from the company Netatmo, which produces intelligent home devices. One of its featured products

267 is the *Smart Home Weather Station*, a portable instrument that measures indoor and outdoor environments.  
268 The users are advised to position the outdoor module half way up the north facing wall of the house, away  
269 from any disturbing heating source and avoiding direct sunlight (Netatmo, 2012). A shield can be purchased  
270 optionally to protect the station from bad weather and sunlight for more reliable readings. Pictures of the device  
271 itself and the shield are provided in SI S2. The outdoor module features an air temperature sensor that has a  
272 measurement range of -40 to 65 °C and accuracy of  $\pm 0.3$  °C. The user can calibrate the temperature manually  
273 by adding an offset. This study utilised the outdoor air temperature measurements shared by Netatmo users  
274 voluntarily. The data were collected from private Netatmo weather stations within the study area via the  
275 Netatmo weather API. A simple quality control of the data combining a simple (Chapman et al., 2017) and an  
276 improved method (Napoly et al., 2018) was conducted by filtering out stations that have the same longitude  
277 and latitude, removing measurements that deviates more than three standard deviations from the average of  
278 measurements from all stations at the same time step, and subsequently discarding data from stations that have  
279 missing values. This resulted in a total of 117 stations with continuous data of good quality within the study  
280 area, covering the period with available meteorological station data. Locations of the meteoblue and Netatmo  
281 stations are shown in Figure 2(a). Measurements were spaced at 30-minute intervals, taken every 15 and 45  
282 minutes after each hour.

## 283 **2.4 Setup and evaluation of TARGET air temperature results**

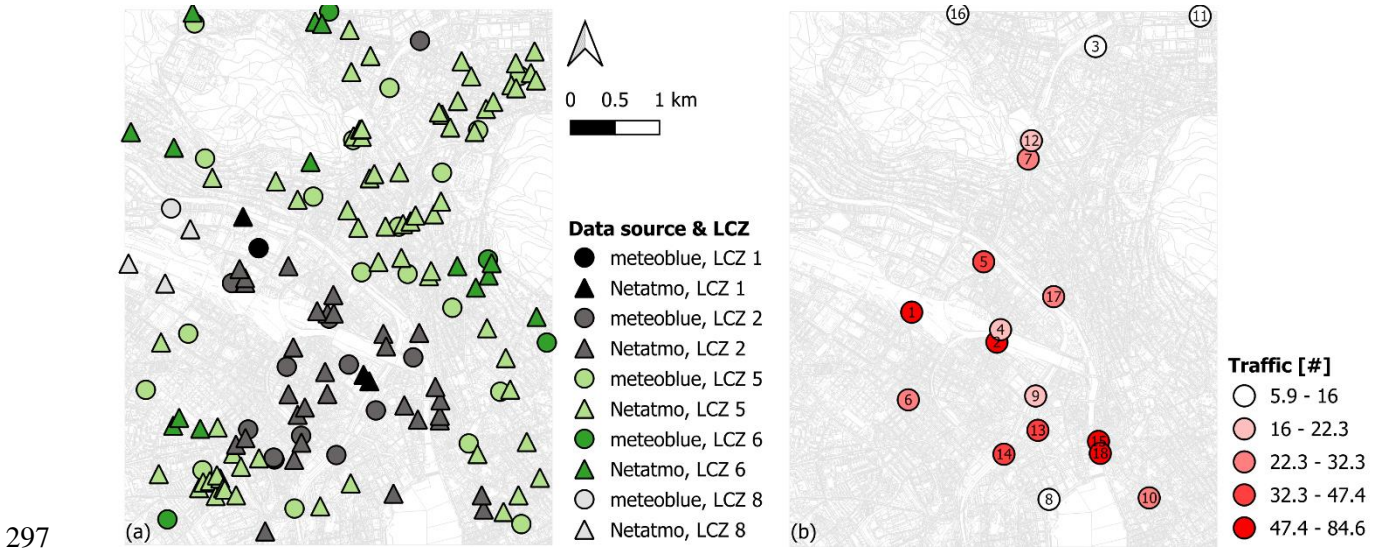
### 284 *2.4.1 Model setup*

285 Surface and air temperatures were simulated with TARGET mainly according to (Broadbent et al., 2019), with  
286 minor changes in LUMPS coefficients as reflected in the most recent version of the model (K. Nice, 2019). A  
287 complete list of parameters used for simulations in this study can be found in Table S3 and the site-specific  
288 values in Table S4 in SI. Simulations covered the period of 2023/07/08 until the beginning of 2023/07/12, the  
289 first 24 hours being the spin-up period.

### 290 *2.4.2 Comparison of TARGET results with spatially distributed observations*

291 As mentioned before, to compare TARGET simulation results with both meteoblue and Netatmo data, we  
292 grouped these weather stations according to the local climate zone they sit in. The modelled results were still  
293 compared to measurements one-to-one for each of the meteoblue or Netatmo data point at every simulation  
294 time step. The grouping is only a measure to investigate how the model performs in different urban  
12

295 environments and does not attempt to mask any errors. The locations and LCZ groups of the stations are shown  
 296 in Figure 2(a).



298 **Figure 2.** Agglomerative clustering of meteoblue and Netatmo stations for model validation (a – left) and average  
 299 hourly pedestrian and bicycle traffic count in the warmer hours (12:00 – 18:00) during the study period (2023/07/09 –  
 300 07/11) at 18 counting stations (labelled as 1 – 18) in the study area (b – right).

### 301 2.5 Sensitivity testing of TARGET

302 A variance-based global sensitivity analysis, or so-called *Sobol sensitivity analysis*, was carried out to better  
 303 understand the TARGET model itself as well as the uncertainty of the modelling results. The Sobol index  
 304 indicates the contribution of variance of a parameter to the output variance. It can be estimated by a quasi-  
 305 Monte Carlo approach, by sampling from parameter ranges, running the sampled values through the model  
 306 and, finally, determining the sensitivity index by calculating estimators (Saltelli et al., 2010; Sobol, 2001).  
 307 Separate indices can be calculated for the first-order effect and higher-order interactions between parameters,  
 308 but this is computationally demanding. Therefore, a total sensitivity index ( $S_T$ ) was used, which measures the  
 309 total contribution of a parameter to the output (Y) variance, including any order effects, which is expressed in  
 310 Equation 8 for parameter i:

$$311 S_{Ti} = 1 - \frac{Var_{X_i}(E_{X_i}(Y|X_i))}{Var(Y)} \quad (8)$$

312 Among TARGET parameters, the four related to the radiative and thermal properties of the surfaces, including  
 313 albedo ( $\alpha$ ), emissivity ( $\epsilon$ ), thermal diffusivity ( $\kappa$ ), and heat capacity (C), were considered worth investigating

314 as they are more accessible for practitioners. We also considered the H/W-ratio of the idealised urban canyon  
 315 in the sensitivity analysis to better understand the important parameters in modelling the urban environment.

316 *Table 1. Parameter ranges for Sobol sensitivity analysis.*

Parameter	Range	Sources
$\alpha_{\text{roof}}$	0.08 – 0.70	(Akbari et al., 1992; Oke, 2002)
$\alpha_{\text{road}}$	0.05 – 0.20	(Akbari et al., 1992; Chartered Institution of Building Services Engineers, 2015; Oke, 2002)
$\alpha_{\text{conc}}$	0.10 – 0.35	(Akbari et al., 1992; Chartered Institution of Building Services Engineers, 2015; Oke, 2002)
$\alpha_{\text{dry}}$	0.19 – 0.32	(Chartered Institution of Building Services Engineers, 2015; Järvi et al., 2011b, 2014)
$\alpha_{\text{irr}}$	0.16 – 0.26	(Barry & Chorley, 2009; Chartered Institution of Building Services Engineers, 2015; Järvi et al., 2011b, 2014; Oke, 2002)
$\alpha_{\text{veg}}$	0.05 – 0.20	(Akbari et al., 1992; Barry & Chorley, 2009; Oke, 2002)
$\epsilon_{\text{roof}}$	0.13 – 1.00	(Bitelli et al., 2015; Oke, 2002)
$\epsilon_{\text{road}}$	0.93 – 0.99	(Bitelli et al., 2015; Oke, 2002)
$\epsilon_{\text{conc}}$	0.80 – 0.98	(Bitelli et al., 2015; Oke, 2002; K. Wang et al., 2005)
$\epsilon_{\text{dry}}$	0.88 – 0.99	(Järvi et al., 2011b, 2014; K. Wang et al., 2005)
$\epsilon_{\text{irr}}$	0.90 – 0.98	(Järvi et al., 2011b, 2014; Oke, 2002; Van Wijk, W. R., Scholte Ubing, 1963)
$\epsilon_{\text{veg}}$	0.97 – 0.99	(Järvi et al., 2011b; Oke, 2002)
$\kappa_{\text{roof}}$	0.05 – 0.57	(Broadbent et al., 2019; Chartered Institution of Building Services Engineers, 2015)
$\kappa_{\text{road}}$	0.29 – 0.62	(Chartered Institution of Building Services Engineers, 2015; Oke, 2002)
$\kappa_{\text{conc}}$	0.08 – 1.51	(Chartered Institution of Building Services Engineers, 2015; Oke, 2002)
$\kappa_{\text{dry}}$	0.11 – 0.32	TARGET default with $\pm 50\%$ variation
$\kappa_{\text{irr}}$	0.21 – 0.63	TARGET default with $\pm 50\%$ variation
$C_{\text{roof}}$	0.81 – 1.96	(Chartered Institution of Building Services Engineers, 2015)
$C_{\text{road}}$	1.70 – 3.91	(Chartered Institution of Building Services Engineers, 2015; Järvi et al., 2011b)
$C_{\text{conc}}$	0.17 – 2.10	(Chartered Institution of Building Services Engineers, 2015)
$C_{\text{dry}}$	0.68 – 2.03	TARGET default with $\pm 50\%$ variation
$C_{\text{irr}}$	1.10 – 3.29	TARGET default with $\pm 50\%$ variation
H/W	0.0015 – 5	Representing nearly open space to extremely dense urban environments

$\alpha$  is the surface albedo,  $\epsilon$  is the surface emissivity,  $\kappa$  is the thermal diffusivity ( $\times 10^{-6}$ ) ( $\text{m}^2 \text{s}^{-1}$ ), and C is the volumetric heat capacity ( $\times 10^6$ ) ( $\text{J m}^{-3} \text{K}^{-1}$ ), H/W is the height-to-width ratio of the idealised urban canyon modelled in TARGET.

317  
 318 The Sobol sensitivity analysis was conducted with a single cell with synthetic land cover input consisting of  
 319 all land cover types in TARGET with equal fractions for a 1-day simulation for 2023/07/09. Variations in  
 320 parameters were limited by their broadest practical ranges, as in Table 1. For cases where there are few  
 321 reference values in the literature, TARGET default values were varied by  $\pm 50\%$ . The Sensitivity Analysis  
 322 Library (SALib) in Python developed by (Herman & Usher, 2017) was utilised for automated analysis. We



323 used a sample size  $N = 1000$  and dimension = 23 for the 23 parameters listed in Table 1. Parameters were  
324 sampled by a quasi-random method (Saltelli et al., 2010) which provides a more uniform coverage of the  
325 parameter space. Average sensitivity over the day, as well as sensitivity indices at three time stamps across the  
326 day, namely 6:00, 14:00 and 22:00, were calculated using Eq. (8), with  $Y$  being the overall average air  
327 temperature (across the study area and study period) and the air temperature at the selected time stamps  
328 averaged over space.

### 329 ***2.6 Evaluation of the impact of blue-green cover on air temperature***

330 An assessment of green and blue cover's impact on air temperature was performed using the simulation results.  
331 The green and blue cover of a grid cell was defined to be the fraction of irrigated grass, trees, and water. Grid  
332 cells were classified according to their green and blue cover (in %) into five groups and the simulated air  
333 temperatures for each group at 6:00, 14:00 and 22:00 on 2023/07/09 were compared using boxplots. The same  
334 analysis for surface temperature was performed to complement the results. We also conducted a multiple linear  
335 regression (ordinary least squares) to calculate the relationship between land cover characteristics and peak air  
336 temperature variability in the study area. Fractions of irrigated grass, trees, and water, separately, were used as  
337 the predictor variables and the dependent variable is the air temperature at 14:00 in each model grid cell.

### 338 ***2.7 Combined consideration of temperature, blue-green cover and pedestrian traffic volume***

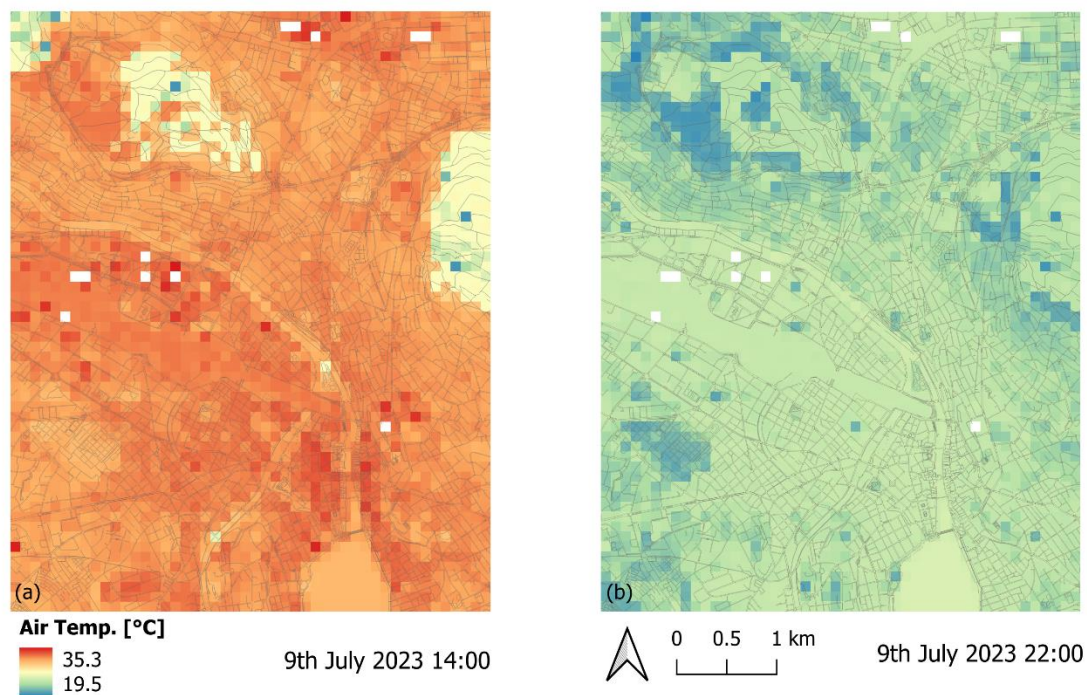
339 The spatial pedestrian and bicycle traffic data made it possible to prioritise locations within the study area by  
340 combining the local air temperature, blue-green cover and the busyness. TARGET-modelled air temperatures  
341 at the 18 locations of the traffic counting stations at the hottest time point (14:00) on 2023/09/07 were extracted  
342 from the simulation results. The blue-green cover for the corresponding model grid cells were taken from the  
343 land cover input and plotted together with air temperature and traffic count data to investigate the impact of  
344 greenery on air temperature at sites travelled more frequently and potential for planning heat mitigation  
345 strategies.

## 346 **3. RESULTS AND DISCUSSION**

### 347 ***3.1 Evaluation of model performance against measurement data***

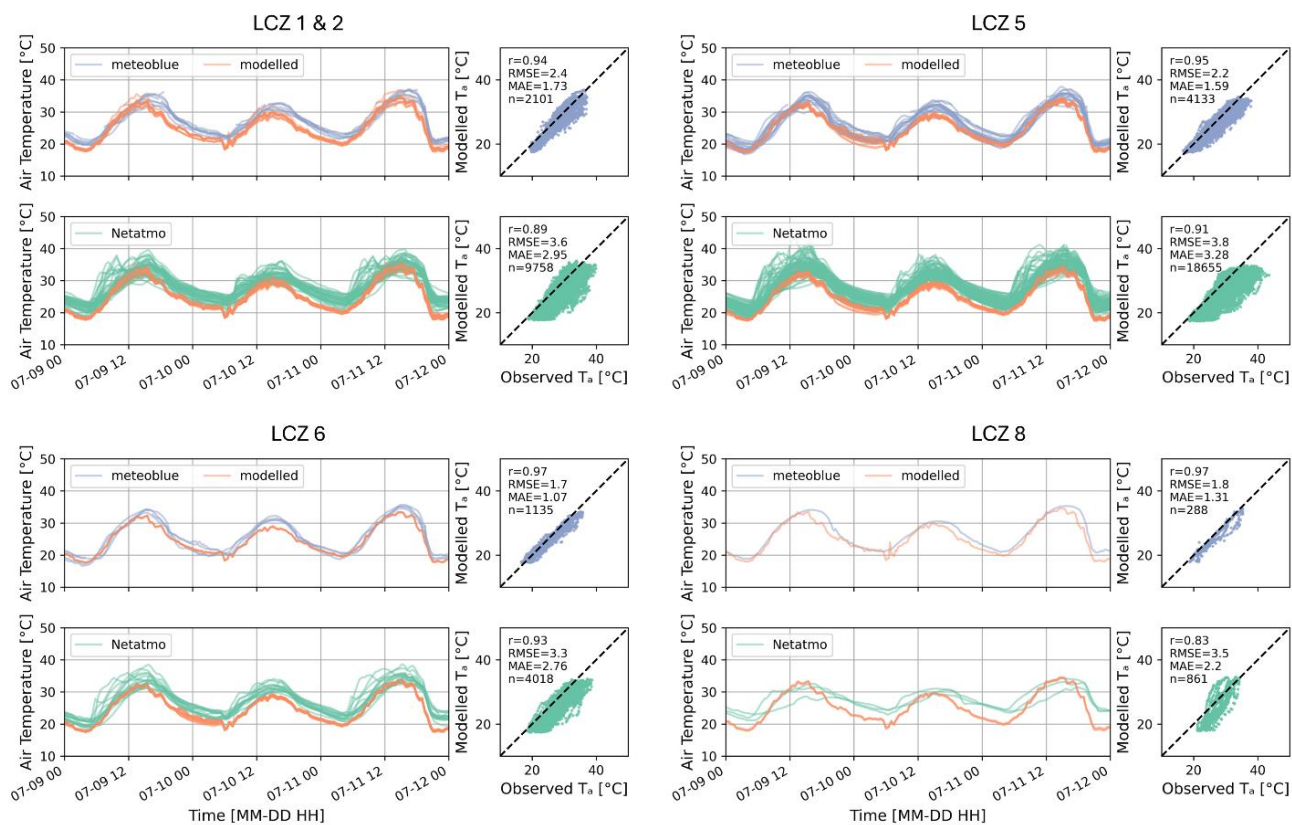
348 Figure 3 demonstrates the spatial distribution of TARGET modelled air temperatures at two points in time, at  
349 14:00 and 22:00. The spatial variations are expected: in the afternoon the densely built urban areas are the

350 warmest, and it is cool in the two forested areas, while at night areas that are open and less urban are the coolest,  
351 water being a bit warmer than other surfaces. Figure 4 shows the validation of the model for different LCZ  
352 groups.  
353



354  
355 **Figure 3.** TARGET modelled air temperature maps (a - left) at 14:00 and (b - right) at 22:00 on 09/07/2023. White  
356 areas are cells with a fraction of roof surface higher than 0.75, for which the air temperature was not calculated by  
357 TARGET.

358 The model generally follows the observed patterns closely, taking meteoblue measurements as representative  
359 of the reality. A lag in air temperature change is observed in densely built areas, when compared with modelling  
360 results. This lag becomes less prominent with increasing vegetation cover and decreasing building heights as  
361 in LCZs 5 and 6, which could be explained by not considering processes of the heat storage and release of  
362 urban surfaces in TARGET. Nevertheless, the model still captures the general spatial and temporal patterns of  
363 air temperature well, achieving an overall correlation coefficient ( $r$ ) of 0.95 and an RMSE of 2.2 °C. An all-  
364 station point-to-point comparison is provided in Figure S7 in SI.



365

366 **Figure 4.** Comparison of the time series of meteoblue (in purple) and Netatmo (in green) air temperature observations  
 367 and TARGET modelled air temperature results (in orange) for weather stations sitting in different LCZs. Observed vs.  
 368 modelled air temperatures are plotted on the right;  $r$  is the correlation coefficient, RMSE is the root mean square error  
 369 [°C], and MAE is the mean absolute error [°C].

370 The five LCZ classes present in Figure 2(a) shows a variation of urban environments in the study area from  
 371 compact high- to mid-rise (LCZs 1 and 2) to open mid- to low- rise (LCZs 5 and 6), where more vegetation is  
 372 present, and large low-rise (LCZ 8), where the land cover is mostly paved. For LCZs 1 and 8 significantly less  
 373 data (4 stations in each LCZ) were available; as such, in the results presented in Figure 4 LCZs 1 and 2 were  
 374 merged but LCZ 8 was kept individually for its lack of similarity to the other classes.

375 Comparing the results for the four groups in Figure 4, we observed a slight increase in model accuracy ( $r =$   
 376 0.94 to 0.97, RMSE = 2.4 to 1.7 °C, MAE = 1.73 to 1.07 °C), comparing against meteoblue data, when the  
 377 urban environment changes from dense buildings to more open arrangements with higher pervious cover.  
 378 Similar trend is seen in the results for Netatmo stations, with some deterioration in the performance indicators,  
 379 which could be explained by the high underlying uncertainty in crowd-sourced data. Higher model accuracy  
 380 for LCZs 5, 6 and 8 might be attributed to higher presence of these LCZ classes in the validation during the  
 17

381 development of the TARGET model, for which data from part of Melbourne (mainly LCZs 6: open low-rise,  
382 8: large low-rise, 4: open high-rise) for land cover surface temperature, and Mawson Lakes (LCZ 8: large low-  
383 rise) for canyon surface and air temperature. Another possible reason of such differences in space is that  
384 elevations are not considered in TARGET and the model was validated in a flat urban area, while Zurich  
385 presents a more hilly landscape. The meteorological station, where the forcing data to drive the model was  
386 from, is located approximately 150 m higher than the lowest areas in the middle of the study area where most  
387 of the LCZs 1 and 2 stations are located. This may explain why the model underestimates the air temperature  
388 the most in the first group and improves as the terrain ascends gradually for LCZs 5 and 6. The same applies  
389 for LCZ 8 as this group is the farthest away from the meteorological, where the conditions could differ.  
390 Considering the lack of elevation in the representation, the validation results are considered good comparing  
391 to the values ( $r = 0.92$ ,  $RMSE = 2.0$  °C) reported in the original TARGET study (Broadbent et al., 2019) and  
392 a more complex model SURFEX ( $r = 0.94 - 0.95$ ,  $RMSE = 1.6 - 1.8$  °C) (Broadbent, Coutts, Tapper, &  
393 Demuzere, 2018) given the simplicity of the model and the comparative nature of the subsequent analyses.  
394 Future studies using the model should consider using different meteorological forcings that are representative  
395 of different areas, or correcting the modelling results according to elevations.

396 Comparing measurement data from the two sources, it is obvious that simple quality control could not improve  
397 the quality of Netatmo data to the same standard as meteoblue data. Netatmo stations measures warmer daytime  
398 temperatures and features a faster warm-up in the morning, which are also seen in (Potgieter et al., 2021),  
399 mostly due to the sitting of the stations. Rigorous quality control and filtering methods are yet to be developed  
400 to make better use of crowdsourced data (Middel et al., 2022). However, the validation using Netatmo data  
401 shows similar trend that was seen in results with meteoblue data, only with deteriorated goodness of fit.  
402 Crowdsourced data can still be useful for model validation and other analysis that requires high-resolution  
403 spatial atmospheric data, especially when the network is dense and confidence can be increased by averaging.

404

### 405 ***3.2 Sensitivity testing results***

406 Sensitivity analysis with 22 radiative and thermal parameters for different surfaces plus the H/W-ratio of the  
407 canyon shows that the H/W-ratio is dominating in modelling the physics of urban canyon compared to other

408 parameters analysed (see SI S6). The simultaneous change of parameters has led to a maximum variation in  
409 the predicted daily and domain average air temperature of 3.6 °C.

410 We therefore repeated the analysis, leaving out the H/W-ratio, to investigate which land cover types are more  
411 important for urban heat. The sensitivity analysis for the 22 physical parameters showed that the heat capacity  
412 and thermal diffusivity of concrete are the most sensitive. This indicates that the heat stored in impervious  
413 surfaces like concrete is a major contributor to urban heat, confirming the findings from a previous study that  
414 daytime air temperature is strongly driven by street fractions (K. A. Nice et al., 2022). A closer look into  
415 sensitivities at different time points revealed that, other than concrete parameters, higher sensitivity was found  
416 in the thermal properties of dry grass for predicting air temperature in early morning. However, the maximum  
417 variation in the average model output when varying these 22 parameters is only 0.07 °C, which is negligible.  
418 Since the H/W-ratio is strictly speaking a model input that is calculated based on building geometry data, we  
419 believe that it is safe to assume typical values for urban surfaces if these modelling parameters are unknown  
420 for a city.

421 It is worth noting that we consider the physical properties for each surface type individually, so the sensitivity  
422 results are limited to the realistic ranges of the parameters for every single surface type. Therefore, these results  
423 might not be able to reflect the general importance of a parameter of the overall built environment, such as the  
424 average albedo for a neighborhood, although it is well known that albedo is an important factor influencing  
425 urban heat (Krayenhoff et al., 2021; L. Wang & Li, 2021).

426 We have also tested the impact of using input data from different meteorological stations on the modelled air  
427 temperature. It was found that stations closer to the study area represents the meteorological conditions within  
428 the region better, especially at night-time; More details on these analyses are presented in SI S5.

429

### 430 ***3.3 Impact of blue-green cover on urban heat***

431 Figure 5(a) displays the influence of blue-green cover on TARGET surface temperature estimations at different  
432 times of the day. The surface temperature difference across different blue-green covers is largest, around 17 °C,  
433 in the afternoon. The median surface temperature decreases as blue-green cover increases. This negative  
434 relationship is also found in the morning and at night, but with less variability. The significant difference in

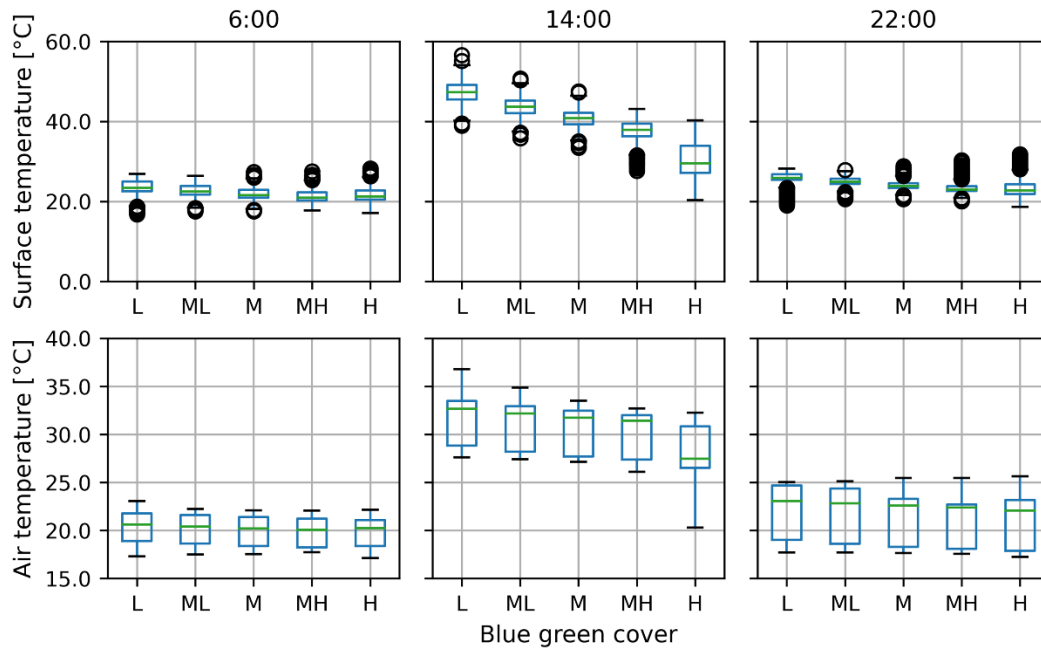
435 surface temperatures represents a reduction of around 5.2 °C in air temperature in the afternoon by increasing  
436 the blue-green cover from low to high, as depicted in Figure (b).

437 Previous studies have found surface temperature reductions of 9 – 19 °C provided by green parks (Wong et al.,  
438 2021), 11.1 °C by artificial lakes and wetlands (Broadbent, Coutts, Tapper, Demuzere, et al., 2018), and air  
439 temperature reductions of 5 °C by water bodies (Murakawa et al., 1991; Peng et al., 2020), 1 – 2 °C provided  
440 by urban green spaces (Aram et al., 2019), which is also supported by more recent studies (Cheung et al., 2021;  
441 Cheung, Jim, et al., 2022; Cheung, Nice, et al., 2022). Our results are on the right end or even beyond these  
442 ranges, because the study area include two large forested areas, *Käferberg* and *Zürichberg*, as described in  
443 Section 2.2. These two areas are in fact very different in terms of land cover compositions, compared to mixed  
444 urban areas. They consist of over 90% trees, meaning that radiation reaching the ground level is substantially  
445 limited. In addition, as the model adds under trees surfaces that are representative of the grid cell land cover  
446 composition, additional cooling is expected when the grid cell has high irrigated grass or water fractions other  
447 than trees. Therefore, the results show a sudden decrease in surface and air temperatures when increasing the  
448 blue-green cover from medium high (MH) to high (H), where all of these forest grid cells belong. If the trend  
449 continues without the sudden decrease, the resulting reductions will be well within the reported ranges in the  
450 previous studies. The large temperature reductions by trees are expected as studies have shown that urban  
451 parks can reduce the air temperature by 0.94 – 5.7 °C (Probst et al., 2022), and that large urban forest can  
452 provide a cooling effect of up to 8.4 °C (Yin et al., 2022). Additionally, elevation can also be an influencing  
453 factor here, as the degree of greenness is apparently related to the topography of the city. Hence, these locations  
454 experience a “double” cooling effect, which can be a reason for the large temperature reductions.

455 The outliers in surface temperature results can be explained by presence of trees together with other blue-green  
456 land covers, which will lead to additional blue-green fractions (bottom outliers), and presence of water (top  
457 outliers). Most of the water surfaces present in the study area are natural deep water bodies (*Lake Zurich* and  
458 *Limmat* river), violating TARGET’s assumption that water depth is within 1 m. The model sometimes  
459 overestimates the air temperature above water, which adds uncertainty to the results.

460 To summarise, the differences between our modelled results and some of the findings in the literature can be  
461 explained by model simplification, different climatic conditions, urban morphology, and urban fabric

462 compositions. Nevertheless, the results show the cooling potential of increasing blue-green cover in urban  
 463 areas, and that our modelling approach can provide reasonable comparisons of different planning scenarios.  
 464



465  
 466 **Figure 5.** Boxplots of modelled (upper) surface temperature and (lower) air temperature for grid cells grouped by blue-  
 467 green cover (L: low, 0-20%, ML: medium low, 20-40%, M: medium, 40-60%, MH: medium high, 60-80%, H: high, 80-  
 468 100%) at 6:00, 14:00, 22:00 for 2023/07/09 to 2023/07/11.

469 To quantify how blue-green land covers contribute to peak air temperature variability, we conducted a multiple  
 470 linear regression of fractions of irrigated grass, trees and water, and the results are shown in Table 2. The  
 471 statistical analysis suggests that trees have the largest impact among the three land cover types, which confirms  
 472 with the results in Figure 5 where temperature drops significantly when large amounts of trees are present.  
 473 Trees are about two times as effective as irrigated grass in providing cooling, while irrigated grass and water  
 474 have similar impacts. However, the cooling impact of water is likely underestimated because of the issue with  
 475 the TARGET water sub-model assumption discussed before.

476 **Table 2.** Peak daytime air temperature multiple linear regression model results.

Variable	Coefficient [°C]	Standard error	t value	p value
Intercept	31.99	0.04	721.56	0.000
% irrigated grass	-2.25	0.12	-19.68	0.000

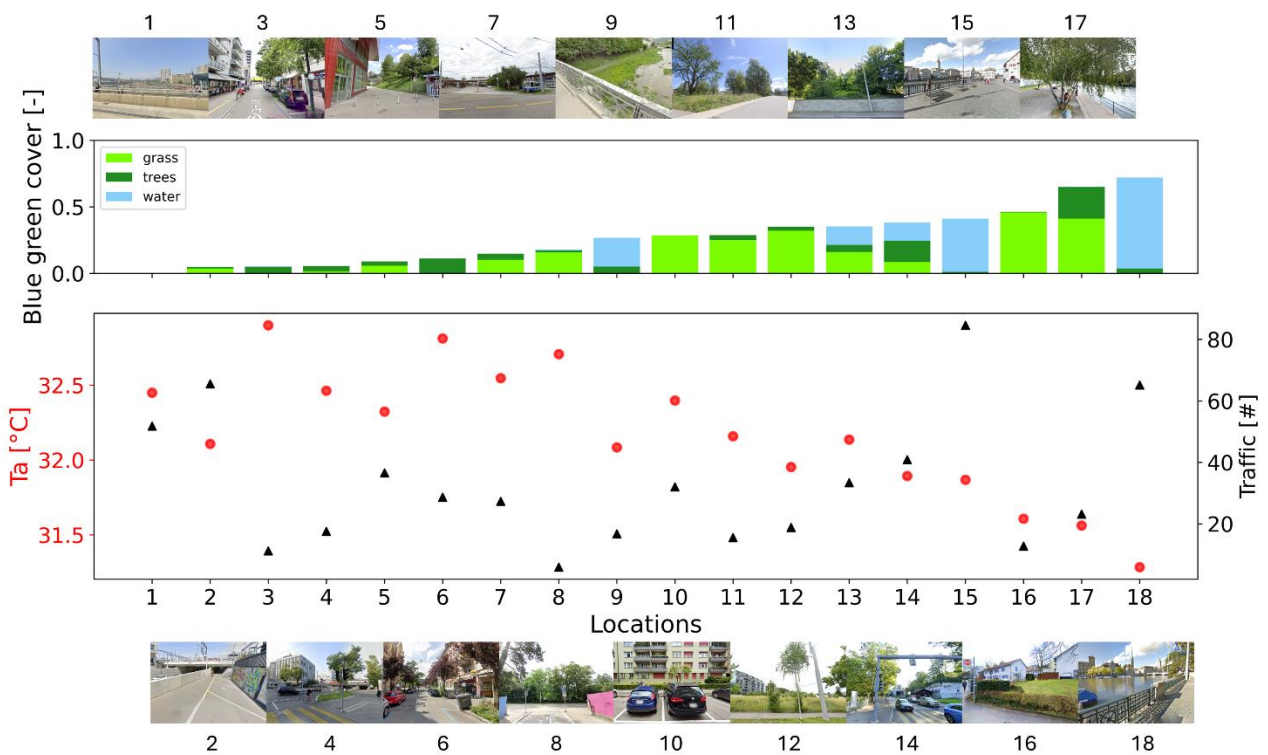
% trees	-4.68	0.10	-47.20	0.000
% water	-2.08	0.17	-12.4	0.000

477 The kind of analysis presented in this section can help practitioners understand approximately how much  
478 cooling impacts they can expect from each type of blue or green land cover in their particular geographical  
479 location. This prior knowledge may assist them in designing urban blue and green spaces more effectively.

#### 480 ***3.4 Investigating modelled spatial cooling effects of urban greenery and blue spaces***

481 Figure 6 incorporates the blue-green cover, air temperature and pedestrian traffic busyness at 18 locations  
482 across the City of Zurich at 14:00 on a warm day (2023/07/09), and demonstrates how TARGET can be used  
483 to pinpoint priority areas for increasing urban greenery. Places with high blue-green cover unsurprisingly  
484 exhibit lower temperatures compared to those with less green and blue spaces. For example, in Figure 6,  
485 location 18 is on a footpath next to the *Limmat* river very close to the city centre. Blue-green cover here is over  
486 70%, and modelled air temperature is 1.6 °C lower than that on a street leading to the train station in the main  
487 commercial area in the district (location 3), where only around 5% street trees are present and the land surface  
488 consists mainly of asphalt and concrete. . A decreasing trend in air temperature is observed with increasing  
489 blue-green cover, and the negative relationship becomes stronger with higher presence of green and blue spaces,  
490 as the modelled air temperature is also influenced by types of impervious land covers that are not shown in  
491 this figure. These impervious land covers play an important role as well. It is not always true that places with  
492 green and blue features have lower temperatures than those without. For instance, a location with 30% greenery  
493 and 70% concrete might be warmer than a location with 100% dry grass.





494

495 **Figure 6.** TARGET modelled air temperatures(extracted from simulation results) at locations 1 – 18 where pedestrian  
 496 traffic count data are available. The locations are ranked according to their blue-green cover, distinguishing between  
 497 fractions of irrigated grass, trees and water. Street views at these locations are from Google Maps.

498 Based on this type of analysis, urban planners can quickly spot places for improvements from temperature  
 499 profiles like those presented in Figure 6. Places with high pedestrian and bicycle traffic volume and low blue-  
 500 green cover are those to be prioritised. To illustrate this idea, location 7 is near *Bucheggplatz*, a transportation  
 501 hub in Zurich, and it would largely benefit commuters and nearby residents if the pervious cover surrounding  
 502 the hub can be increased. Another example is location 6 in a rather densely built residential area. Despite some  
 503 trees on sides of the street, this place appears to have a higher temperature than most of the other locations.  
 504 Although it can be challenging to alter the land surface considering the already tight space, improvements  
 505 should certainly be sought. The same applies to location 2 on *Langstrasse*, one of the liveliest streets in the  
 506 city. Identifying locations like these forms a starting point for urban planners to develop plans and assess  
 507 proposed greening options by modifying the land cover and simulating new modelling conditions. They can  
 508 even plan for connected green spaces along the routes and throughout the city to maximise cooling  
 509 (Gunawardena et al., 2017; Zhang et al., 2017).

510 As the placement of green features is found to be more opportunistic than strategically planned (Kuller et al.,  
511 2021), and planning practitioners are willing to adopt novel planning tools (Kuller et al., 2022), TARGET,  
512 together with post-spatial analysis, can fit in this purpose very well. The methods we proposed and  
513 demonstrated in this study are easy to adopt, fast to process, and operable at a city-scale. The model is also  
514 highly flexible to simulate the cooling impact of different greenery options including types, locations and even  
515 maintenance level (by switching between dry and wet grass), under different climate conditions (past, present  
516 or future) and in different places. Modelling results can be coupled with different data, not necessarily traffic,  
517 to evaluate heat mitigation options with consideration of other factors according to user preferences. It is also  
518 possible to implement a multi-criteria decision analysis (MCDA) approach starting with the idea presented in  
519 this paper.

### 520 ***3.5 Limitations of the proposed approach***

521 We demonstrated a range of applications that TARGET can be used to support the planning of urban  
522 microclimate. Although TARGET was the specific tool used, the overall methodology could utilise any  
523 suitable simplified climate model. Nevertheless, several limitations remain that future work can address.

524 TARGET's design represents a trade-off between speed and level of detail to support planners in evaluating  
525 suburb- to city-scale blue-green infrastructure solutions and test heat mitigation scenarios. As such, it aims to  
526 generate reliable temperature estimations while maintaining computational efficiency and consequently makes  
527 several key assumptions. One crucial assumption of TARGET is that it does not consider horizontal advection  
528 (Broadbent et al., 2019). In reality, the local cooling impact of these infrastructures is weakened by atmospheric  
529 mixing, which is particularly strong when wind speed is high (Broadbent et al., 2019). Without proper  
530 representation of the horizontal mixing of air in the model, the predicted cooling benefits of greenery in this  
531 study would most likely be the maximum value.

532 In addition, as mentioned before, the water sub-model of TARGET is not designed for natural lakes and rivers,  
533 which were present in the case study; this sometimes leads to instability in the air temperature results above  
534 these water surfaces. Variation of elevation is not accounted for in the model. This simplification could lead  
535 to errors in air temperature results for the case study. These are limitations we acknowledge and worked with  
536 throughout our analysis.

#### 537 4. CONCLUSION

538 This study reports insights into modelling air temperature with an urban climate model called TARGET to  
539 assess the impacts of green and blue spaces and plan liveable cities. We compared TARGET results with local  
540 air temperature measurements from professional climate service and data provider and crowd-sourced data  
541 from home devices, and also conducted a parameter sensitivity analysis for the model. Finally, we  
542 demonstrated how TARGET results can be used to support spatial planning of green and blue spaces in cities  
543 to improve city liveability. The study found that city-wide modelling with TARGET generally captures the air  
544 temperature patterns well ( $r = 0.95$ ,  $RMSE = 2.2^{\circ}C$ ). Additionally, we demonstrated the added value of  
545 spatially distributed temperature data from private sensor networks to validate urban climate models. Based  
546 on the sensitivity testing results, the canyon height-to-width ratio was found to be the most influential on urban  
547 heat, and concrete parameters had more impact on the results than other surfaces' parameters. Application of  
548 the model to the case study of Zurich found that an air temperature reduction of around  $1.2^{\circ}C$  can be achieved  
549 by increasing the blue-green cover of a location from low (0 – 20%) to medium high (60 – 80%), and a further  
550  $4^{\circ}C$  if the location is transformed to an urban forest, which are in accordance with literature values and  
551 confirms the validity of the predicted cooling impact provided by increasing green and blue spaces. Notably,  
552 we showed that TARGET is useful for identifying critical locations for urban heat mitigation when coupled  
553 with spatial pedestrian count data.

554 In summary, we found that TARGET is a useful tool to simulate air temperature fast and accurately at city-  
555 scale, allowing urban planners to: (1) identify locations for improvements by looking for low blue-green cover  
556 and high temperature, (2) assess different planning options simply by altering the land covers and run TARGET  
557 with the new land cover input, (3) couple TARGET results with different spatial data for multi-faceted analyses.  
558 The framework around quick and efficient model setup and simulation we presented in this study is  
559 generalisable to other locations and offers opportunity for urban planners to use simplified models for  
560 improving the liveability in cities.

561

562 *Code and data availability.* TARGET is distributed under the Creative Commons Attribution-  
563 NonCommercial-ShareAlike 4.0 Generic (CC BY-NC-SA 4.0). Python code used for this study is available at  
564 <https://github.com/jixuan-chen/target>.

565

## 566 **ACKNOWLEDGEMENTS**

567 This work was funded by the Swiss National Science Foundation (SNSF) Project 200021\_201029: *Heat-Down*  
568 – *Integrated Modelling of Stormwater and Urban Heat for cooling Cities*. We would also like to thank  
569 Christian Förster for his assistance in scripts for the data mining of crowd-sourced temperature measurements.

570 **REFERENCES**

- 571 Akbari, H., Davis, S., Dorsano, S., Huang, J., & Winnett, S. (Eds.). (1992). *Cooling our Communities—A*  
572 *Guidebook On Tree Planting And Light Colored Surfacing*. US Environmental Protection Agency.
- 573 Alves, F. M., Gonçalves, A., & Del Caz-Enjuto, M. R. (2022). The Use of Envi-Met for the Assessment of  
574 Nature-Based Solutions' Potential Benefits in Industrial Parks—A Case Study of Argales Industrial  
575 Park (Valladolid, Spain). *Infrastructures*, 7(6), 85. <https://doi.org/10.3390/infrastructures7060085>
- 576 Amt für Raumentwicklung Zürich. (2019). *AV - Bodenbedeckung*.
- 577 Anders, J., Schubert, S., Sauter, T., Tunn, S., Schneider, C., & Salim, M. (2023). Modelling the impact of an  
578 urban development project on microclimate and outdoor thermal comfort in a mid-latitude city. *Energy*  
579 *and Buildings*, 296, 113324. <https://doi.org/10.1016/j.enbuild.2023.113324>
- 580 Aram, F., Higuera García, E., Solgi, E., & Mansournia, S. (2019). Urban green space cooling effect in cities.  
581 *Heliyon*, 5(4), e01339. <https://doi.org/10.1016/j.heliyon.2019.e01339>
- 582 Ballester, J., Quijal-Zamorano, M., Méndez Turrubiates, R. F., Pegenaute, F., Herrmann, F. R., Robine, J. M.,  
583 Basagaña, X., Tonne, C., Antó, J. M., & Achebak, H. (2023). Heat-related mortality in Europe during  
584 the summer of 2022. *Nature Medicine*. <https://doi.org/10.1038/s41591-023-02419-z>
- 585 Barry, R. G., & Chorley, R. J. (2009). *Atmosphere, Weather and Climate* (8th ed.). Routledge.
- 586 Bitelli, G., Conte, P., Csoknyai, T., Franci, F., Girelli, V. A., & Mandanici, E. (2015). Aerial thermography  
587 for energetic modelling of cities. *Remote Sensing*, 7(2), 2152–2170.  
588 <https://doi.org/10.3390/rs70202152>
- 589 Bouzouidja, R., Cannavo, P., Bodéan, P., Gulyás, Á., Kiss, M., Kovács, A., Béchet, B., Chancibault, K.,  
590 Chantoiseau, E., Bournet, P.-E., Bouzidi, R., Guénon, R., Lebeau, T., Musy, M., & Rodriguez, F.  
591 (2021). How to evaluate nature-based solutions performance for microclimate, water and soil  
592 management issues – Available tools and methods from Nature4Cities European project results.  
593 *Ecological Indicators*, 125, 107556. <https://doi.org/10.1016/j.ecolind.2021.107556>
- 594 Broadbent, A. M., Coutts, A. M., Nice, K. A., Demuzere, M., Krayenhoff, E. S., Tapper, N. J., & Wouters, H.  
595 (2019). The Air-temperature Response to Green/blue-infrastructure Evaluation Tool (TARGET v1.0):

596 An efficient and user-friendly model of city cooling. *Geoscientific Model Development*, 12(2), 785–  
597 803. <https://doi.org/10.5194/gmd-12-785-2019>

598 Broadbent, A. M., Coutts, A. M., Tapper, N. J., & Demuzere, M. (2018). The cooling effect of irrigation on  
599 urban microclimate during heatwave conditions. *Urban Climate*, 23, 309–329.  
600 <https://doi.org/10.1016/j.uclim.2017.05.002>

601 Broadbent, A. M., Coutts, A. M., Tapper, N. J., Demuzere, M., & Beringer, J. (2018). The microscale cooling  
602 effects of water sensitive urban design and irrigation in a suburban environment. *Theoretical and  
603 Applied Climatology*, 134(1–2), 1–23. <https://doi.org/10.1007/s00704-017-2241-3>

604 Bruse, M., & Fleer, H. (1998). Simulating surface-plant-air interactions inside urban environments with a three  
605 dimensional numerical model. *Environmental Modelling and Software*, 13(3–4), 373–384.  
606 [https://doi.org/10.1016/S1364-8152\(98\)00042-5](https://doi.org/10.1016/S1364-8152(98)00042-5)

607 Bueno, B., Norford, L., Hidalgo, J., & Pigeon, G. (2013). The urban weather generator. *Journal of Building  
608 Performance Simulation*, 6(4), 269–281. <https://doi.org/10.1080/19401493.2012.718797>

609 Chapman, L., Bell, C., & Bell, S. (2017). Can the crowdsourcing data paradigm take atmospheric science to a  
610 new level? A case study of the urban heat island of London quantified using Netatmo weather stations.  
611 *International Journal of Climatology*, 37(9), 3597–3605. <https://doi.org/10.1002/joc.4940>

612 Chartered Institution of Building Services Engineers. (2015). *Environmental Design: CIBSE Guide A*. CIBSE.

613 Cheung, P. K., Jim, C. Y., Tapper, N., Nice, K. A., & Livesley, S. J. (2022). Daytime irrigation leads to  
614 significantly cooler private backyards in summer. *Urban Climate*, 46, 101310.  
615 <https://doi.org/10.1016/j.uclim.2022.101310>

616 Cheung, P. K., Livesley, S. J., & Nice, K. A. (2021). Estimating the cooling potential of irrigating green spaces  
617 in 100 global cities with arid, temperate or continental climates. *Sustainable Cities and Society*, 71,  
618 102974. <https://doi.org/10.1016/j.scs.2021.102974>

619 Cheung, P. K., Nice, K. A., & Livesley, S. J. (2022). Irrigating urban green space for cooling benefits: The  
620 mechanisms and management considerations. *Environmental Research: Climate*, 1(1), 015001.  
621 <https://doi.org/10.1088/2752-5295/ac6e7c>

622 Copernicus. (2024, September 6). *Copernicus: Summer 2024 – Hottest on record globally and for Europe*.  
623 <https://climate.copernicus.eu/copernicus-summer-2024-hottest-record-globally-and-europe>

- 624 Demuzere, M., Kittner, J., Martilli, A., Mills, G., Moede, C., Stewart, I. D., van Vliet, J., & Bechtel, B. (2022).  
625 A global map of local climate zones to support earth system modelling and urban-scale environmental  
626 science. *Earth System Science Data*, *14*(8), 3835–3873. <https://doi.org/10.5194/essd-14-3835-2022>
- 627 Ebi, K. L., Capon, A., Berry, P., Broderick, C., de Dear, R., Havenith, G., Honda, Y., Kovats, R. S., Ma, W.,  
628 Malik, A., Morris, N. B., Nybo, L., Seneviratne, S. I., Vanos, J., & Jay, O. (2021). Hot weather and  
629 heat extremes: Health risks. *The Lancet*, *398*(10301), 698–708. [https://doi.org/10.1016/S0140-](https://doi.org/10.1016/S0140-6736(21)01208-3)  
630 [6736\(21\)01208-3](https://doi.org/10.1016/S0140-6736(21)01208-3)
- 631 Elraouf, R. A., ELMokadem, A., Megahed, N., Eleinen, O. A., & Eltarabily, S. (2022). Evaluating urban  
632 outdoor thermal comfort: A validation of ENVI-met simulation through field measurement. *Journal*  
633 *of Building Performance Simulation*, *15*(2), 268–286.  
634 <https://doi.org/10.1080/19401493.2022.2046165>
- 635 García-León, D., Casanueva, A., Standardi, G., Burgstall, A., Flouris, A. D., & Nybo, L. (2021). Current and  
636 projected regional economic impacts of heatwaves in Europe. *Nature Communications*, *12*(1), 5807.  
637 <https://doi.org/10.1038/s41467-021-26050-z>
- 638 Geletič, J., Lehnert, M., Krč, P., Resler, J., & Krayenhoff, E. S. (2021). High-Resolution Modelling of Thermal  
639 Exposure during a Hot Spell: A Case Study Using PALM-4U in Prague, Czech Republic. *Atmosphere*,  
640 *12*(2), 175. <https://doi.org/10.3390/atmos12020175>
- 641 Gobatti, L., Bach, P. M., Scheidegger, A., & Leitão, J. P. (2023). Using satellite imagery to investigate Blue-  
642 Green Infrastructure establishment time for urban cooling. *Sustainable Cities and Society*, *97*, 104768.  
643 <https://doi.org/10.1016/j.scs.2023.104768>
- 644 Grimmond, C. S. B., & Oke, T. R. (1991). An evapotranspiration-interception model for urban areas. *Water*  
645 *Resources Research*, *27*(7), 1739–1755. <https://doi.org/10.1029/91WR00557>
- 646 Grimmond, C. S. B., & Oke, T. R. (2002). Turbulent Heat Fluxes in Urban Areas: Observations and a Local-  
647 Scale Urban Meteorological Parameterization Scheme (LUMPS). *Journal of Applied Meteorology*,  
648 *41*(7), 792–810. [https://doi.org/10.1175/1520-0450\(2002\)041<0792:THFIUA>2.0.CO;2](https://doi.org/10.1175/1520-0450(2002)041<0792:THFIUA>2.0.CO;2)
- 649 Gromke, C., Blocken, B., Janssen, W., Merema, B., van Hooff, T., & Timmermans, H. (2015). CFD analysis  
650 of transpirational cooling by vegetation: Case study for specific meteorological conditions during a

651 heat wave in Arnhem, Netherlands. *Building and Environment*, 83, 11–26.  
652 <https://doi.org/10.1016/j.buildenv.2014.04.022>

653 Gunawardena, K. R., Wells, M. J., & Kershaw, T. (2017). Utilising green and bluespace to mitigate urban heat  
654 island intensity. *Science of The Total Environment*, 584–585, 1040–1055.  
655 <https://doi.org/10.1016/j.scitotenv.2017.01.158>

656 Herman, J., & Usher, W. (2017). SALib: An open-source Python library for Sensitivity Analysis. *The Journal*  
657 *of Open Source Software*, 2(9), 97. <https://doi.org/10.21105/joss.00097>

658 IPCC. (2021). *Climate change 2021: The physical science basis. Contribution of Working Group I to the Sixth*  
659 *Assessment Report of the Intergovernmental Panel on Climate Change*. Cambridge University Press  
660 Cambridge, UK.

661 IPCC. (2022). *Summary for Policymakers*. Cambridge University Press.  
662 [https://www.ipcc.ch/report/ar6/wg2/downloads/report/IPCC\\_AR6\\_WGII\\_SummaryForPolicymakers](https://www.ipcc.ch/report/ar6/wg2/downloads/report/IPCC_AR6_WGII_SummaryForPolicymakers)  
663 .pdf

664 Jacobs, A. F. G., Heusinkveld, B. G., & Berkowicz, S. M. (2000). Force-restore technique for ground surface  
665 temperature and moisture content in a dry desert system. *Water Resources Research*, 36(5), 1261–  
666 1268. <https://doi.org/10.1029/2000WR900016>

667 Jamei, E., Seyedmahmoudian, M., Horan, B., & Stojcevski, A. (2019). Verification of a bioclimatic modeling  
668 system in a growing suburb in Melbourne. *Science of the Total Environment*, 689, 883–898.  
669 <https://doi.org/10.1016/j.scitotenv.2019.06.399>

670 Järvi, L., Grimmond, C. S. B., & Christen, A. (2011a). The Surface Urban Energy and Water Balance Scheme  
671 (SUEWS): Evaluation in Los Angeles and Vancouver. *Journal of Hydrology*, 411(3–4), 219–237.  
672 <https://doi.org/10.1016/j.jhydrol.2011.10.001>

673 Järvi, L., Grimmond, C. S. B., & Christen, A. (2011b). The Surface Urban Energy and Water Balance Scheme  
674 (SUEWS): Evaluation in Los Angeles and Vancouver. *Journal of Hydrology*, 411(3–4), 219–237.  
675 <https://doi.org/10.1016/j.jhydrol.2011.10.001>

676 Järvi, L., Grimmond, C. S. B., Taka, M., Nordbo, A., Setälä, H., & Strachan, I. B. (2014). Development of the  
677 Surface Urban Energy and Water Balance Scheme (SUEWS) for cold climate cities. *Geoscientific*  
678 *Model Development*, 7(4), 1691–1711. <https://doi.org/10.5194/gmd-7-1691-2014>



- 679 Jia, S., & Wang, Y. (2021). Effect of heat mitigation strategies on thermal environment, thermal comfort, and  
680 walkability: A case study in Hong Kong. *Building and Environment*, 201, 107988.  
681 <https://doi.org/10.1016/j.buildenv.2021.107988>
- 682 Krayenhoff, E. S., Broadbent, A. M., Zhao, L., Georgescu, M., Middel, A., Voogt, J. A., Martilli, A., Sailor,  
683 D. J., & Erell, E. (2021). Cooling hot cities: A systematic and critical review of the numerical  
684 modelling literature. *Environmental Research Letters*, 16(5), 053007. [https://doi.org/10.1088/1748-  
685 9326/abdcf1](https://doi.org/10.1088/1748-9326/abdcf1)
- 686 Kuller, M., Farrelly, M., Marthanty, D. R., Deletic, A., & Bach, P. M. (2022). Planning support systems for  
687 strategic implementation of nature-based solutions in the global south: Current role and future  
688 potential in Indonesia. *Cities*, 126, 103693. <https://doi.org/10.1016/j.cities.2022.103693>
- 689 Kuller, M., Reid, D. J., & Prodanovic, V. (2021). Are we planning blue-green infrastructure opportunistically  
690 or strategically? Insights from Sydney, Australia. *Blue-Green Systems*, 3(1), 267–280.  
691 <https://doi.org/10.2166/bgs.2021.023>
- 692 Kwok, Y. T., & Ng, E. Y. Y. (2021). Trends, topics, and lessons learnt from real case studies using mesoscale  
693 atmospheric models for urban climate applications in 2000–2019. *Urban Climate*, 36, 100785.  
694 <https://doi.org/10.1016/j.uclim.2021.100785>
- 695 Lindberg, F., Grimmond, C. S. B., & Martilli, A. (2015). Sunlit fractions on urban facets – Impact of spatial  
696 resolution and approach. *Urban Climate*, 12, 65–84. <https://doi.org/10.1016/j.uclim.2014.11.006>
- 697 Lindberg, F., Holmer, B., & Thorsson, S. (2008). SOLWEIG 1.0—Modelling spatial variations of 3D radiant  
698 fluxes and mean radiant temperature in complex urban settings. *International Journal of  
699 Biometeorology*, 52(7), 697–713. <https://doi.org/10.1007/s00484-008-0162-7>
- 700 Manoli, G., Fatichi, S., Schläpfer, M., Yu, K., Crowther, T. W., Meili, N., Burlando, P., Katul, G. G., & Bou-  
701 Zeid, E. (2019). Magnitude of urban heat islands largely explained by climate and population. *Nature*,  
702 573(7772), 55–60. <https://doi.org/10.1038/s41586-019-1512-9>
- 703 Maronga, B., Banzhaf, S., Burmeister, C., Esch, T., Forkel, R., Fröhlich, D., Fuka, V., Gehrke, K. F., Geletič,  
704 J., Giersch, S., Gronemeier, T., Groß, G., Heldens, W., Hellsten, A., Hoffmann, F., Inagaki, A.,  
705 Kadasch, E., Kanani-Sühring, F., Ketelsen, K., ... Raasch, S. (2020). Overview of the PALM model

706 system 6.0. *Geoscientific Model Development*, 13(3), 1335–1372. [https://doi.org/10.5194/gmd-13-](https://doi.org/10.5194/gmd-13-1335-2020)  
707 1335-2020

708 Masson, V. (2000). A Physically-Based Scheme For The Urban Energy Budget In Atmospheric Models.  
709 *Boundary-Layer Meteorology*, 94(3), 357–397. <https://doi.org/10.1023/A:1002463829265>

710 Masson, V., Lemonsu, A., Hidalgo, J., & Voogt, J. (2020). Urban Climates and Climate Change. *Annual*  
711 *Review of Environment and Resources*, 45(1), 411–444. [https://doi.org/10.1146/annurev-environ-](https://doi.org/10.1146/annurev-environ-012320-083623)  
712 012320-083623

713 Matsson, J. E. (2023). *An introduction to ansys fluent 2023*. Sdc Publications.

714 Matzarakis, A., Rutz, F., & Mayer, H. (2007). Modelling radiation fluxes in simple and complex  
715 environments—Application of the RayMan model. *International Journal of Biometeorology*, 51(4),  
716 323–334. <https://doi.org/10.1007/s00484-006-0061-8>

717 Meili, N., Manoli, G., Burlando, P., Bou-Zeid, E., Chow, W. T. L., Coutts, A. M., Daly, E., Nice, K. A., Roth,  
718 M., Tapper, N. J., Velasco, E., Vivoni, E. R., & Fatichi, S. (2020). An urban ecohydrological model  
719 to quantify the effect of vegetation on urban climate and hydrology (UT&C v1.0). *Geoscientific Model*  
720 *Development*, 13(1), 335–362. <https://doi.org/10.5194/gmd-13-335-2020>

721 meteoblue. (2024). *Measure urban climate where it matters with modern IoT technology*. Meteoblue.  
722 [https://content.meteoblue.com/en/business-solutions/meteo-climate-services/city-climate/iot-station-](https://content.meteoblue.com/en/business-solutions/meteo-climate-services/city-climate/iot-station-network/)  
723 [network/](https://content.meteoblue.com/en/business-solutions/meteo-climate-services/city-climate/iot-station-network/)

724 MeteoSwiss. (2023). *Automatic measurement network*.  
725 [https://www.meteoswiss.admin.ch/weather/measurement-systems/land-based-stations/automatic-](https://www.meteoswiss.admin.ch/weather/measurement-systems/land-based-stations/automatic-measurement-network.html)  
726 [measurement-network.html](https://www.meteoswiss.admin.ch/weather/measurement-systems/land-based-stations/automatic-measurement-network.html)

727 Middel, A., Nazarian, N., Demuzere, M., & Bechtel, B. (2022). Urban Climate Informatics: An Emerging  
728 Research Field. *Frontiers in Environmental Science*, 10. <https://doi.org/10.3389/fenvs.2022.867434>

729 Middel, A., Turner, V. K., Schneider, F. A., Zhang, Y., & Stiller, M. (2020). Solar reflective pavements—A  
730 policy panacea to heat mitigation? *Environmental Research Letters*, 15(6), 064016.  
731 <https://doi.org/10.1088/1748-9326/ab87d4>

- 732 Mortezaazadeh, M., Wang, L. L., Albettar, M., & Yang, S. (2022). CityFFD – City fast fluid dynamics for urban  
733 microclimate simulations on graphics processing units. *Urban Climate*, *41*, 101063.  
734 <https://doi.org/10.1016/j.uclim.2021.101063>
- 735 Mouada, N., Zemmouri, N., & Meziani, R. (2019). Urban morphology, outdoor thermal comfort and  
736 walkability in hot, dry cities: Case study in Sidi Okba, Algeria. *International Review for Spatial  
737 Planning and Sustainable Development*, *7*(1), 117–133. [https://doi.org/10.14246/irspsda.7.1\\_117](https://doi.org/10.14246/irspsda.7.1_117)
- 738 Murakawa, S., Sekine, T., Narita, K., & Nishina, D. (1991). Study of the effects of a river on the thermal  
739 environment in an urban area. *Energy and Buildings*, *16*(3), 993–1001. [https://doi.org/10.1016/0378-  
740 7788\(91\)90094-J](https://doi.org/10.1016/0378-7788(91)90094-J)
- 741 Musy, M., Malys, L., Morille, B., & Inard, C. (2015). The use of SOLENE-microclimat model to assess  
742 adaptation strategies at the district scale. *Urban Climate*, *14*, 213–223.  
743 <https://doi.org/10.1016/j.uclim.2015.07.004>
- 744 Napoly, A., Grassmann, T., Meier, F., & Fenner, D. (2018). Development and Application of a Statistically-  
745 Based Quality Control for Crowdsourced Air Temperature Data. *Frontiers in Earth Science*, *6*.  
746 <https://www.frontiersin.org/articles/10.3389/feart.2018.00118>
- 747 Nazarian, N., Krayenhoff, E. S., Bechtel, B., Hondula, D. M., Paolini, R., Vanos, J., Cheung, T., Chow, W. T.  
748 L., de Dear, R., Jay, O., Lee, J. K. W., Martilli, A., Middel, A., Norford, L. K., Sadeghi, M., Schiavon,  
749 S., & Santamouris, M. (2022). Integrated Assessment of Urban Overheating Impacts on Human Life.  
750 *Earth's Future*, *10*(8), e2022EF002682. <https://doi.org/10.1029/2022EF002682>
- 751 Netatmo. (2012). *Netatmo user manual*. [https://static.netatmo.com/station/faq\\_en-US.pdf](https://static.netatmo.com/station/faq_en-US.pdf)
- 752 Nice, K. (2019). *Mothlight / target\_java*. *Bitbucket Repository*.  
753 [https://bitbucket.org/mothlight/target\\_java/src/master/](https://bitbucket.org/mothlight/target_java/src/master/)
- 754 Nice, K. A., Coutts, A. M., & Tapper, N. J. (2018). Development of the VTUF-3D v1.0 urban micro-climate  
755 model to support assessment of urban vegetation influences on human thermal comfort. *Urban Climate*,  
756 *24*, 1052–1076. <https://doi.org/10.1016/j.uclim.2017.12.008>
- 757 Nice, K. A., Nazarian, N., Lipson, M. J., Hart, M. A., Seneviratne, S., Thompson, J., Naserikia, M., Godic, B.,  
758 & Stevenson, M. (2022). Isolating the impacts of urban form and fabric from geography on urban heat

759 and human thermal comfort. *Building and Environment*, 224, 109502.  
760 <https://doi.org/10.1016/j.buildenv.2022.109502>

761 Nicholls, N., Skinner, C., Loughnan, M., & Tapper, N. (2008). A simple heat alert system for Melbourne,  
762 Australia. *International Journal of Biometeorology*, 52(5), 375–384. [https://doi.org/10.1007/s00484-](https://doi.org/10.1007/s00484-007-0132-5)  
763 [007-0132-5](https://doi.org/10.1007/s00484-007-0132-5)

764 Oke, T. R. (1987). *Boundary layer climates* (Second edition). Routledge.

765 Oke, T. R. (2002). *Boundary Layer Climates*. (2nd ed.). Routledge.

766 Oke, T. R., Mills, G., Christen, A., & Voogt, J. A. (2017). *Urban Climates*. Cambridge University Press.  
767 <https://doi.org/10.1017/9781139016476>

768 Ozkeresteci, I., Crewe, K., Brazel, A. J., & Bruse, M. (2003). *Use and Evaluation of the Envi-Met Model for*  
769 *Environmental Design and Planning: An Experiment on Linear Parks*.

770 Peng, J., Liu, Q., Xu, Z., Lyu, D., Du, Y., Qiao, R., & Wu, J. (2020). How to effectively mitigate urban heat  
771 island effect? A perspective of waterbody patch size threshold. *Landscape and Urban Planning*, 202,  
772 103873. <https://doi.org/10.1016/j.landurbplan.2020.103873>

773 Potgieter, J., Nazarian, N., Lipson, M. J., Hart, M. A., Ulpiani, G., Morrison, W., & Benjamin, K. (2021).  
774 Combining High-Resolution Land Use Data With Crowdsourced Air Temperature to Investigate Intra-  
775 Urban Microclimate. *Frontiers in Environmental Science*, 9, 720323.  
776 <https://doi.org/10.3389/fenvs.2021.720323>

777 Probst, N., Bach, P. M., Cook, L. M., Maurer, M., & Leitão, J. P. (2022). Blue Green Systems for urban heat  
778 mitigation: Mechanisms, effectiveness and research directions. *Blue-Green Systems*, 4(2), 348–376.  
779 <https://doi.org/10.2166/bgs.2022.028>

780 Salata, F., Golasi, I., De Lieto Vollaro, R., & De Lieto Vollaro, A. (2016). Urban microclimate and outdoor  
781 thermal comfort. A proper procedure to fit ENVI-met simulation outputs to experimental data.  
782 *Sustainable Cities and Society*, 26, 318–343. <https://doi.org/10.1016/j.scs.2016.07.005>

783 Saltelli, A., Annoni, P., Azzini, I., Campolongo, F., Ratto, M., & Tarantola, S. (2010). Variance based  
784 sensitivity analysis of model output. Design and estimator for the total sensitivity index. *Computer*  
785 *Physics Communications*, 181(2), 259–270. <https://doi.org/10.1016/j.cpc.2009.09.018>

786 Santamouris, M., & Fiorito, F. (2021). On the impact of modified urban albedo on ambient temperature and  
787 heat related mortality. *Solar Energy*, 216, 493–507. <https://doi.org/10.1016/j.solener.2021.01.031>

788 Schneider, F. A., Ortiz, J. C., Vanos, J. K., Sailor, D. J., & Middel, A. (2023). Evidence-based guidance on  
789 reflective pavement for urban heat mitigation in Arizona. *Nature Communications*, 14(1), 1467.  
790 <https://doi.org/10.1038/s41467-023-36972-5>

791 Skoulika, F., Santamouris, M., Kolokotsa, D., & Boemi, N. (2014). On the thermal characteristics and the  
792 mitigation potential of a medium size urban park in Athens, Greece. *Landscape and Urban Planning*,  
793 123, 73–86. <https://doi.org/10.1016/j.landurbplan.2013.11.002>

794 Sobol, I. M. (2001). Global sensitivity indices for nonlinear mathematical models and their Monte Carlo  
795 estimates. *Mathematics and Computers in Simulation*, 55(1–3), 271–280.  
796 [https://doi.org/10.1016/S0378-4754\(00\)00270-6](https://doi.org/10.1016/S0378-4754(00)00270-6)

797 Solecki, W., & Marcotullio, P. J. (2013). Climate Change and Urban Biodiversity Vulnerability. In T. Elmqvist,  
798 M. Fragkias, J. Goodness, B. Güneralp, P. J. Marcotullio, R. I. McDonald, S. Parnell, M. Schewenius,  
799 M. Sendstad, K. C. Seto, & C. Wilkinson (Eds.), *Urbanization, Biodiversity and Ecosystem Services:  
800 Challenges and Opportunities* (pp. 485–504). Springer Netherlands. [https://doi.org/10.1007/978-94-  
801 007-7088-1\\_25](https://doi.org/10.1007/978-94-007-7088-1_25)

802 Stadt Zürich. (2023). *Daten der automatischen Fussgänger- und Velozählung—Viertelstundenwerte*.  
803 [https://data.stadt-  
804 zuerich.ch/dataset/ted\\_taz\\_verkehrszaehlungen\\_werte\\_fussgaenger\\_velo/resource/8bb6b21f-e412-  
805 4710-a50f-26202b2d1ca3](https://data.stadt-zuerich.ch/dataset/ted_taz_verkehrszaehlungen_werte_fussgaenger_velo/resource/8bb6b21f-e412-4710-a50f-26202b2d1ca3)

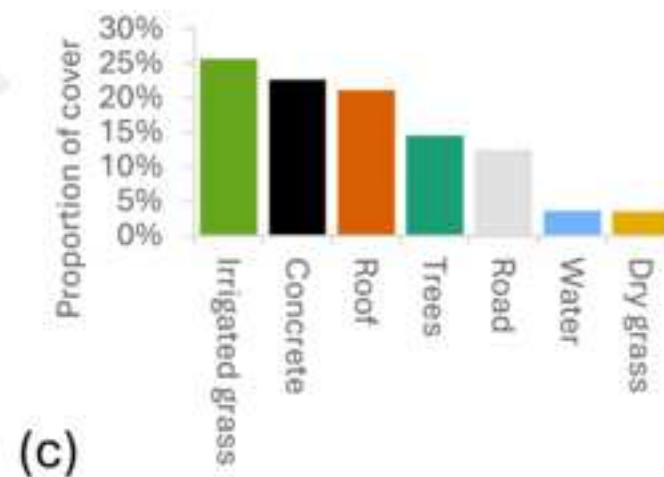
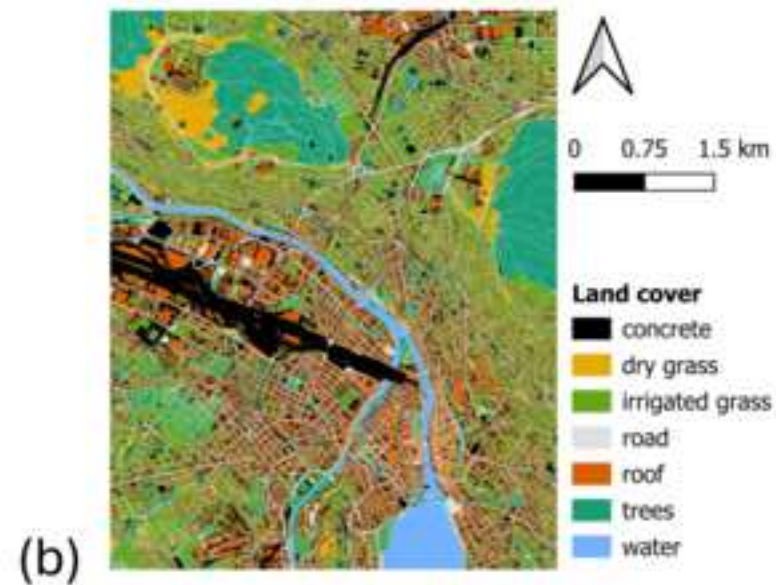
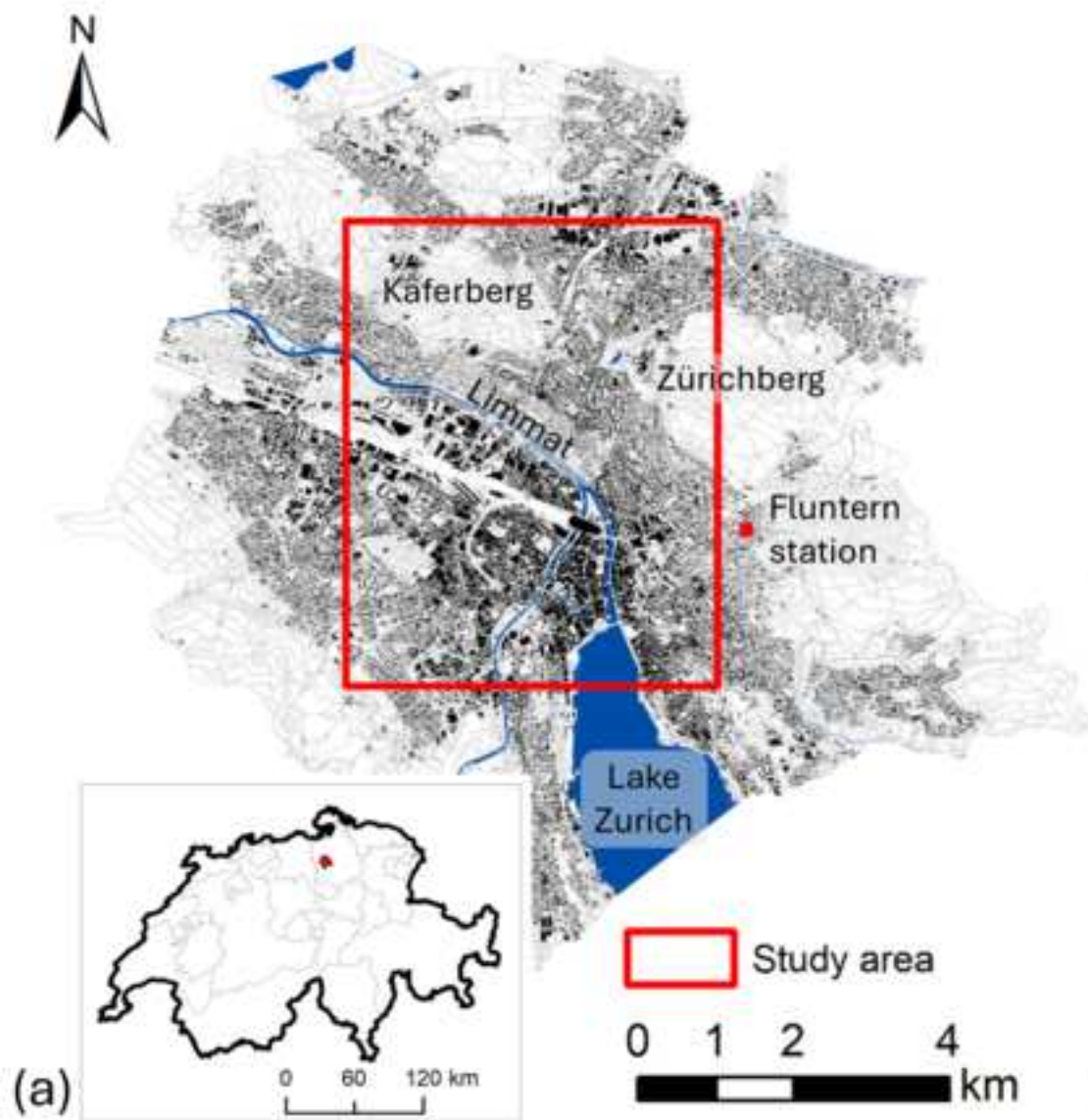
806 swisstopo. (2020). *swissSURFACE3D Raster* [Dataset]. [https://www.swisstopo.admin.ch/en/height-model-  
807 swisssurface3d-raster](https://www.swisstopo.admin.ch/en/height-model-swisssurface3d-raster)

808 Toparlar, Y., Blocken, B., Maiheu, B., & van Heijst, G. J. F. (2017). A review on the CFD analysis of urban  
809 microclimate. *Renewable and Sustainable Energy Reviews*, 80, 1613–1640.  
810 <https://doi.org/10.1016/j.rser.2017.05.248>

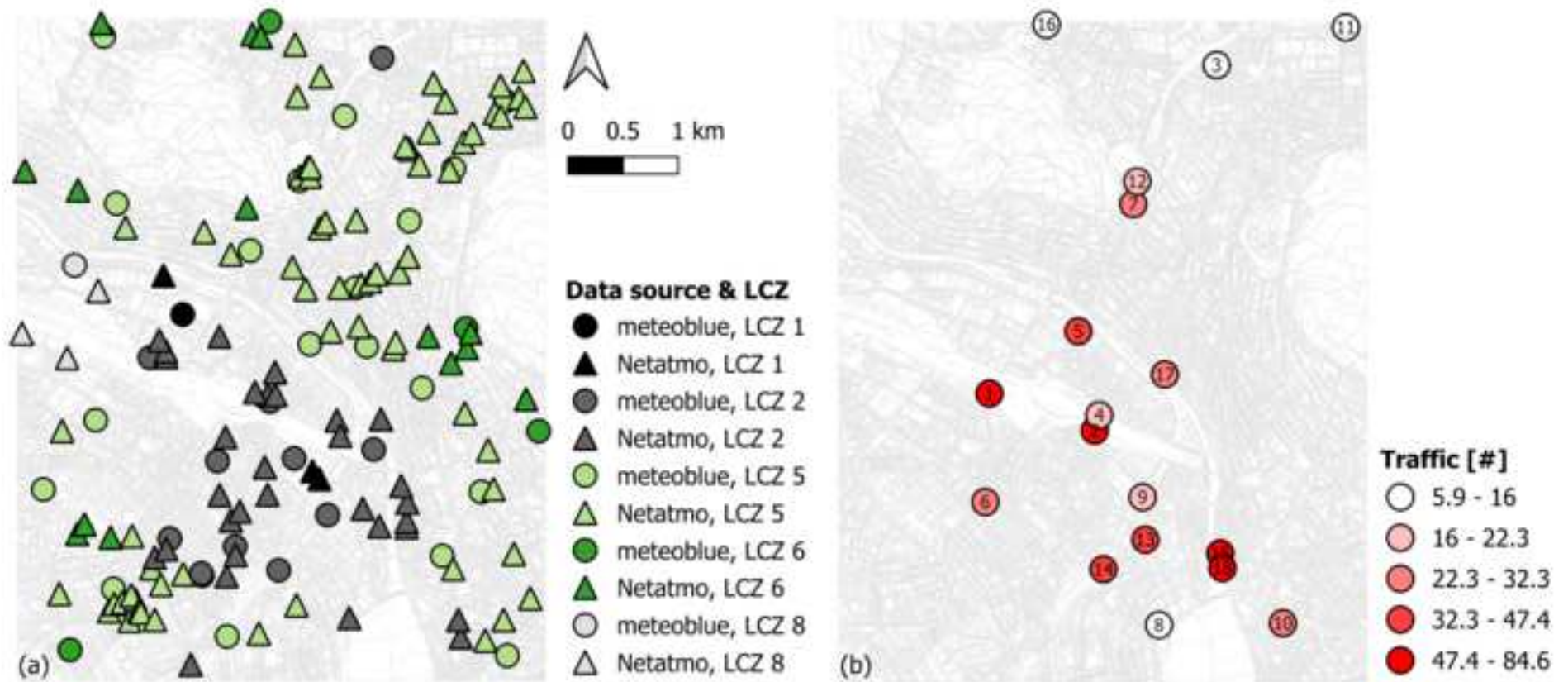
811 Topham, G. (2022, July 19). Why do Britain’s roads melt and its rails buckle in heat? *The Guardian*.  
812 [https://www.theguardian.com/business/2022/jul/19/why-does-britains-tarmac-melt-and-its-rails-  
813 buckle-in-heat](https://www.theguardian.com/business/2022/jul/19/why-does-britains-tarmac-melt-and-its-rails-buckle-in-heat)

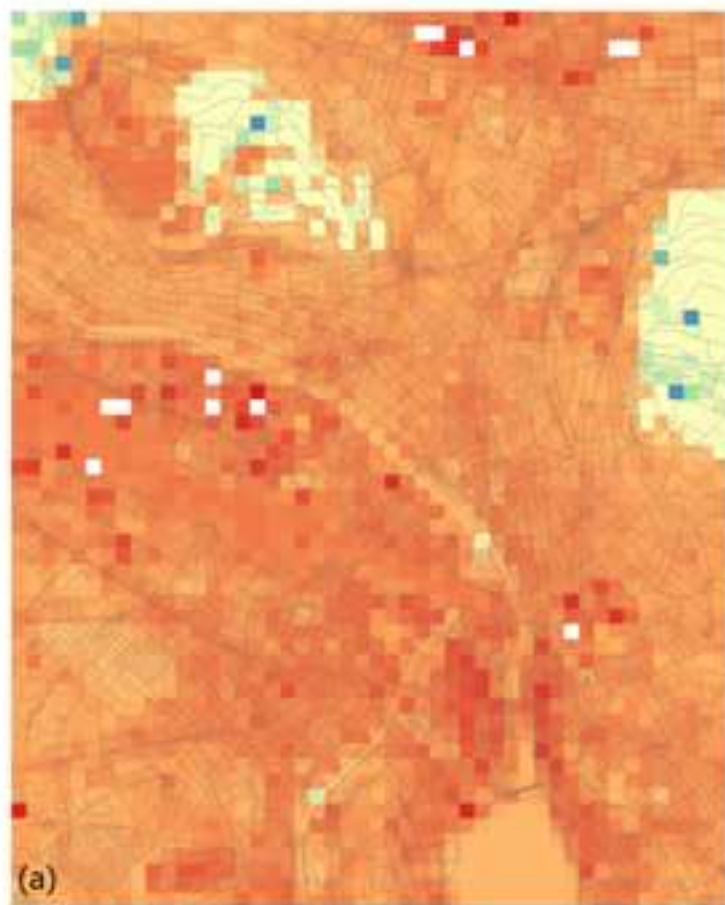
- 814 Tsoka, S., Tsikaloudaki, A., & Theodosiou, T. (2018). Analyzing the ENVI-met microclimate model's  
815 performance and assessing cool materials and urban vegetation applications—A review. *Sustainable*  
816 *Cities and Society*, 43, 55–76. <https://doi.org/10.1016/j.scs.2018.08.009>
- 817 United Nations. (2019). *World Urbanization Prospects The 2018 Revision (ST/ESA/SER.A/420)*. United  
818 Nations, Department of Economic and Social Affairs, Population Division.
- 819 United Nations. (2022, July 19). *WMO warns of frequent heatwaves in decades ahead*. UN News.  
820 <https://news.un.org/en/story/2022/07/1122822>
- 821 Vahmani, P., & Jones, A. D. (2017). Water conservation benefits of urban heat mitigation. *Nature*  
822 *Communications*, 8(1), 1072. <https://doi.org/10.1038/s41467-017-01346-1>
- 823 Van Wijk, W. R., Scholte Ubing, D. W. (1963). Radiation. In *Physics of plant environment* (pp. 62–101).  
824 North-Holland Pub. Co.
- 825 Wang, C., Wang, Z.-H., Kaloush, K. E., & Shacat, J. (2021). Cool pavements for urban heat island mitigation:  
826 A synthetic review. *Renewable and Sustainable Energy Reviews*, 146, 111171.  
827 <https://doi.org/10.1016/j.rser.2021.111171>
- 828 Wang, K., Wan, Z., Wang, P., Sparrow, M., Liu, J., Zhou, X., & Haginoya, S. (2005). Estimation of surface  
829 long wave radiation and broadband emissivity using moderate resolution imaging spectroradiometer  
830 (MODIS) land surface temperature/emissivity products. *Journal of Geophysical Research D:*  
831 *Atmospheres*, 110(11), 1–12. <https://doi.org/10.1029/2004JD005566>
- 832 Wang, L., & Li, D. (2021). *Urban Heat Islands during Heat Waves: A Comparative Study between Boston and*  
833 *Phoenix*. <https://doi.org/10.1175/JAMC-D-20-0132.1>
- 834 Weller, H. G., Tabor, G., Jasak, H., & Fureby, C. (1998). A tensorial approach to computational continuum  
835 mechanics using object-oriented techniques. *Computer in Physics*, 12(6), 620–631.  
836 <https://doi.org/10.1063/1.168744>
- 837 Wong, N. H., Tan, C. L., Kolokotsa, D. D., & Takebayashi, H. (2021). Greenery as a mitigation and adaptation  
838 strategy to urban heat. *Nature Reviews Earth & Environment*, 2(3), 166–181.  
839 <https://doi.org/10.1038/s43017-020-00129-5>

- 840 Yin, S., Peng, L. L. H., Feng, N., Wen, H., Ling, Z., Yang, X., & Dong, L. (2022). Spatial-temporal pattern in  
841 the cooling effect of a large urban forest and the factors driving it. *Building and Environment*, 209,  
842 108676. <https://doi.org/10.1016/j.buildenv.2021.108676>
- 843 Yu, C., & Hien, W. N. (2006). Thermal benefits of city parks. *Energy and Buildings*, 38(2), 105–120.  
844 <https://doi.org/10.1016/j.enbuild.2005.04.003>
- 845 Yu, Z., Guo, X., Jørgensen, G., & Vejre, H. (2017). How can urban green spaces be planned for climate  
846 adaptation in subtropical cities? *Ecological Indicators*, 82, 152–162.  
847 <https://doi.org/10.1016/j.ecolind.2017.07.002>
- 848 Zhang, Y., Murray, A. T., & Turner, B. L. (2017). Optimizing green space locations to reduce daytime and  
849 nighttime urban heat island effects in Phoenix, Arizona. *Landscape and Urban Planning*, 165, 162–  
850 171. <https://doi.org/10.1016/j.landurbplan.2017.04.009>
- 851





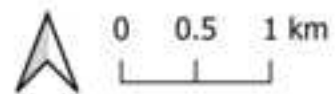




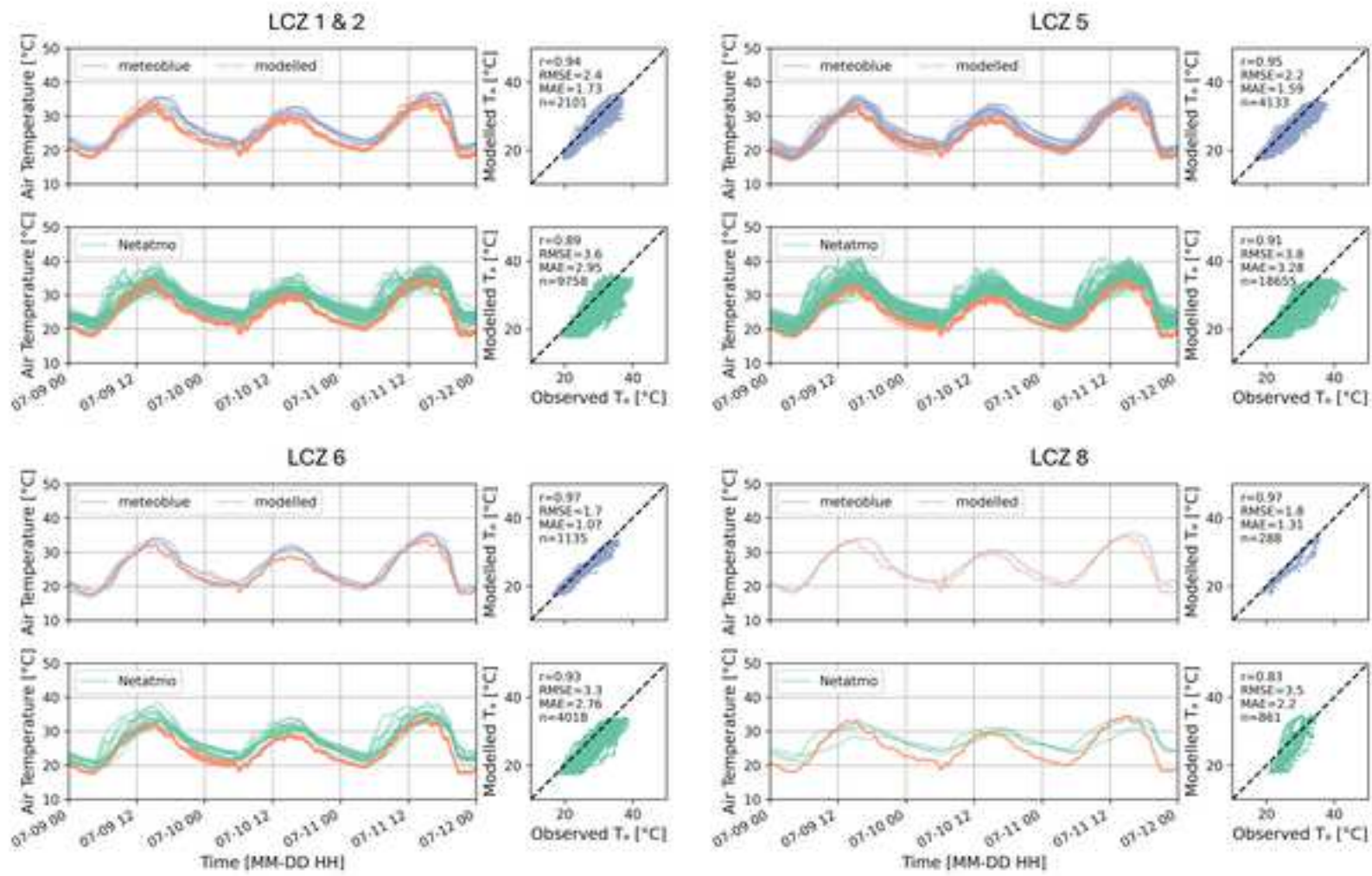
**Air Temp. [°C]**



9th July 2023 14:00



9th July 2023 22:00





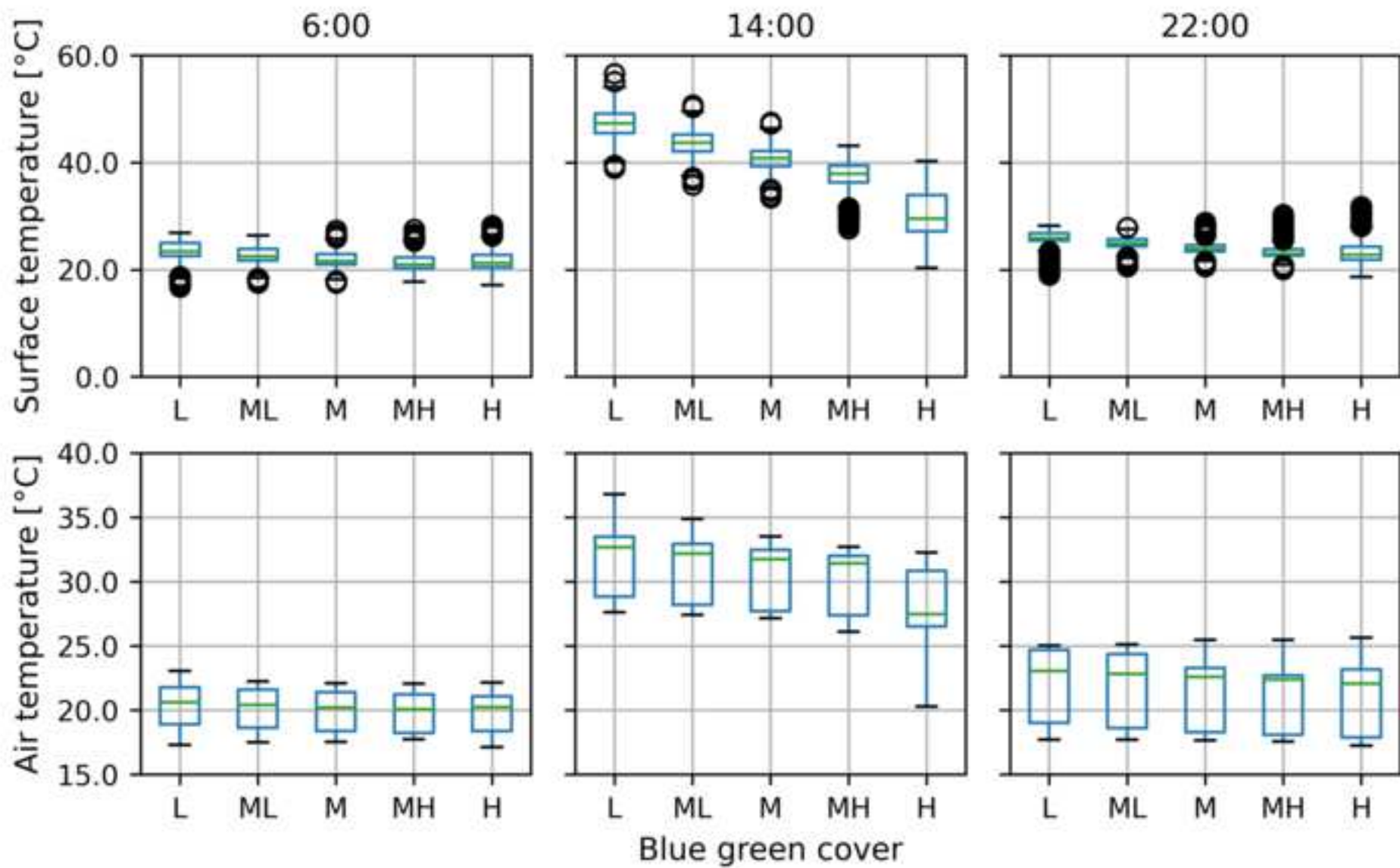
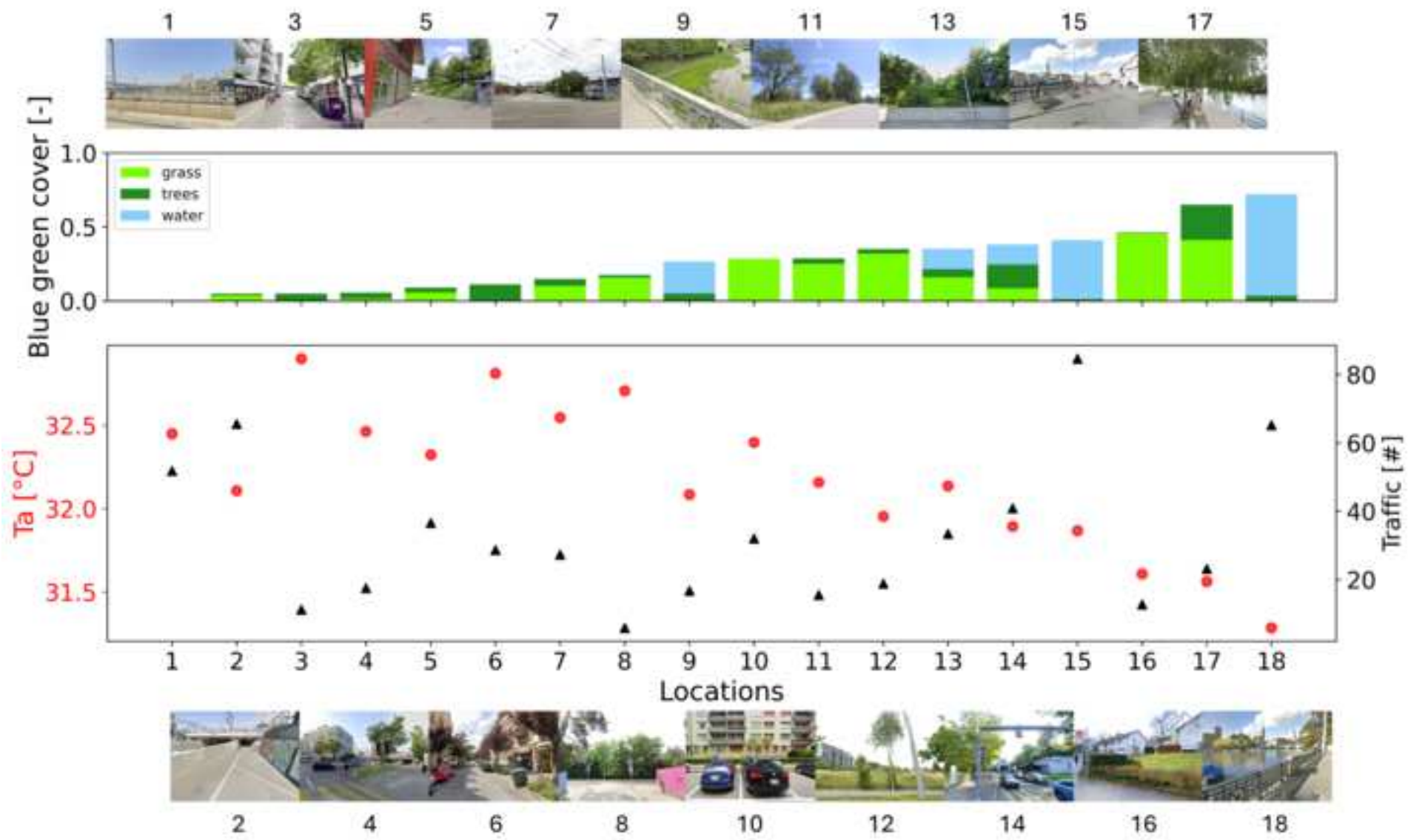


Figure 6





Click here to access/download  
**Supplementary Material**  
Chen et al. supp\_240930.docx

